Hyperspectral Deposit Atlas - Deep Leads

Geological Survey Technical Report TR50

Mineral Resources Tasmania

Tasmanian Government

Geological Survey Technical Report 50:

Hyperspectral Deposit Atlas
Deep Leads

by

J. Moltzen

August 2026

Cover: Easy access for drilling crews on recently-harvested hardwood plantations and farmland (photo courtesy of ABx Group).

Executive Summary

This report summarises results from HyLogger-3 scanning of reverse circulation (RC) drillholes from the Deep Leads clay-hosted rare earth element (REE) deposit. Hyperspectral data are integrated with available geochemical datasets to enhance deposit-scale characterisation and mineralogical and geochemical interpretations.

An analysis of hyperspectral data suggests that REE enrichment is associated with poorly-crystalline kaolinite at the Deep Leads project and with montmorillonite at the Wind Break project. A strong association between goethite and cerium is observed, reflecting oxidative weathering processes that drive the decoupling of cerium from other REEs. Under oxidising conditions, cerium is converted to its less mobile tetravalent form ($Ce^{3+} \rightarrow Ce^{4+}$) and preferentially stabilised within goethite, whereas the more soluble REEs are mobilised and enriched in the saprolite zone.

Prolonged in-situ weathering has produced a well-developed vertical zonation. At Deep Leads, an upper, oxidised and REE-depleted zone is characterised by elevated iron oxide abundance, increased kaolinite crystallinity and a cerium anomaly. A lower zone of REE enrichment is characterised by reduced iron oxide content and the presence of poorly-crystalline kaolinite. At Wind Break, higher proportions of montmorillonite, commonly mixed with nontronite or well-crystalline kaolinite, are observed throughout the saprolite zone associated with REE enrichment.

Deposit-scale analysis demonstrates the effectiveness of hyperspectral techniques in resolving mineralogical controls on REE distribution and regolith zonation. The data confirms that HyLogger can be used to characterise clay mineralogy, identify REE associations, and delineate vertical zonation. This improved understanding has important implications for building robust geological models, developing orebody knowledge, derisking resource estimations, and optimising minerals processing strategies. Based on these findings, we recommend routine hyperspectral core logging using HyLogger as a standard tool for the characterisation and evaluation of clay-hosted REE deposits.

Tasmanian Government

Mineral Resources Tasmania
www.mrt.tas.gov.au

Hyperspectral Deposit Atlas
Deep Leads

by J. Moltzen
Geological Survey Branch - Mineral Resources Tasmania

CONTENTS

FIGURES

TABLES

APPENDICES

1.0 INTRODUCTION

This hyperspectral deposit atlas presents results from HyLogger-3 scanning of reverse circulation (RC) drillholes from ABx Group's Deep Leads clay-hosted rare earth element (REE) deposit. The aim of this atlas is to provide systematic interpretations of hyperspectral data generated through Mineral Resources Tasmania's HyLogger program and to improve understanding of the key geological and mineralogical characteristics of the deposit. To enhance deposit-scale characterisation, spectral data have been integrated with publicly available geochemical datasets, providing a more comprehensive approach for mineralogical and geochemical interpretation.

This study focuses on:

i. characterising the mineralogy and spatial distribution of key mineral phases throughout the deposit
ii. identifying REE–mineral associations, including the occurrence and potential host phases of ionically adsorbed REEs
iii. evaluating clay mineral characteristics and their relationship to REE enrichment, and
iv. defining the vertical weathering profile, with particular emphasis on REE distribution and the development of distinct regolith zones.

Complete HyLogger datasets, including tray imagery and spectral outputs, are released as part of this publication (Appendix A). The framework developed for this atlas is intended for application on future hyperspectral deposit atlas editions targeting other mineral systems in Tasmania. A key objective is to improve the accessibility and geological interpretation of HyLogger outputs, enhancing their application within the Tasmanian minerals industry.

2.0 GEOLOGICAL SETTING

The Deep Leads clay-hosted rare earth element (REE) project is located in northern Tasmania, approximately 40 km west of Launceston (Figure 1), and sits within the Late Carboniferous to Late Triassic Tasmanian Basin. The basin extends across much of central and eastern Tasmania and is stratigraphically divided into the Lower and Upper Parmeener Supergroup. The Lower Parmeener Supergroup comprises a mixed succession of glacial to glaciomarine and non-marine sedimentary rocks, including diamictite, fine-grained sandstone, coarse siltstone, and fossiliferous mudstone (Corbett et al., 2014). The Upper Parmeener Supergroup records a transition to predominantly terrestrial conditions, and comprises coal measures, quartz arenite, quartz sandstone interbedded with mudstone and shale, and feldspathic sandstone.

Basin sequences have been subsequently intruded by Jurassic dolerite, emplaced extensively as part of the widespread magmatic event associated with the breakup of Gondwana (approximately 183 Ma; Ivanov et al., 2016; Ware et al., 2023). These dolerite sheets occur as thick sills (400 – 500 m) intruded between flat lying sediments, form a significant component of the basin architecture and presently occupy most of the outcropping area throughout the region (Seymour and Calver, 1995). Cenozoic volcanic rocks, predominantly alkali basalts, erupted during more recent intraplate volcanic activity and are most extensively distributed in the northwestern region of Tasmania, with several flows mapped throughout the basin (Everard et al., 2024). Both dolerite and basalt provide a key source of primary minerals, including mafic silicates and accessory phases capable of hosting rare earth elements and are the dominant lithologies encountered at Deep Leads.

3.0 DEEP LEADS

Formation of REE mineralisation at Deep Leads is interpreted to have resulted from prolonged in-situ weathering of Jurassic tholeiitic dolerite and Tertiary alkali basalts under warm temperate climatic conditions (Russo et al., 2025). Established Ionic Adsorption Clay Deposit (IACD) REE formation models have described progressive chemical weathering processes leading to the partial breakdown of primary REE-bearing minerals, facilitating the liberation and mobilisation of REEs (Sanematsu and Watanabe, 2016). These elements are subsequently either incorporated into secondary REE-bearing phases (e.g. rhabdophane and aluminium phosphate–sulphate [APS] minerals) or become ionically adsorbed onto the surfaces of clay minerals, predominantly kaolinite and smectite.

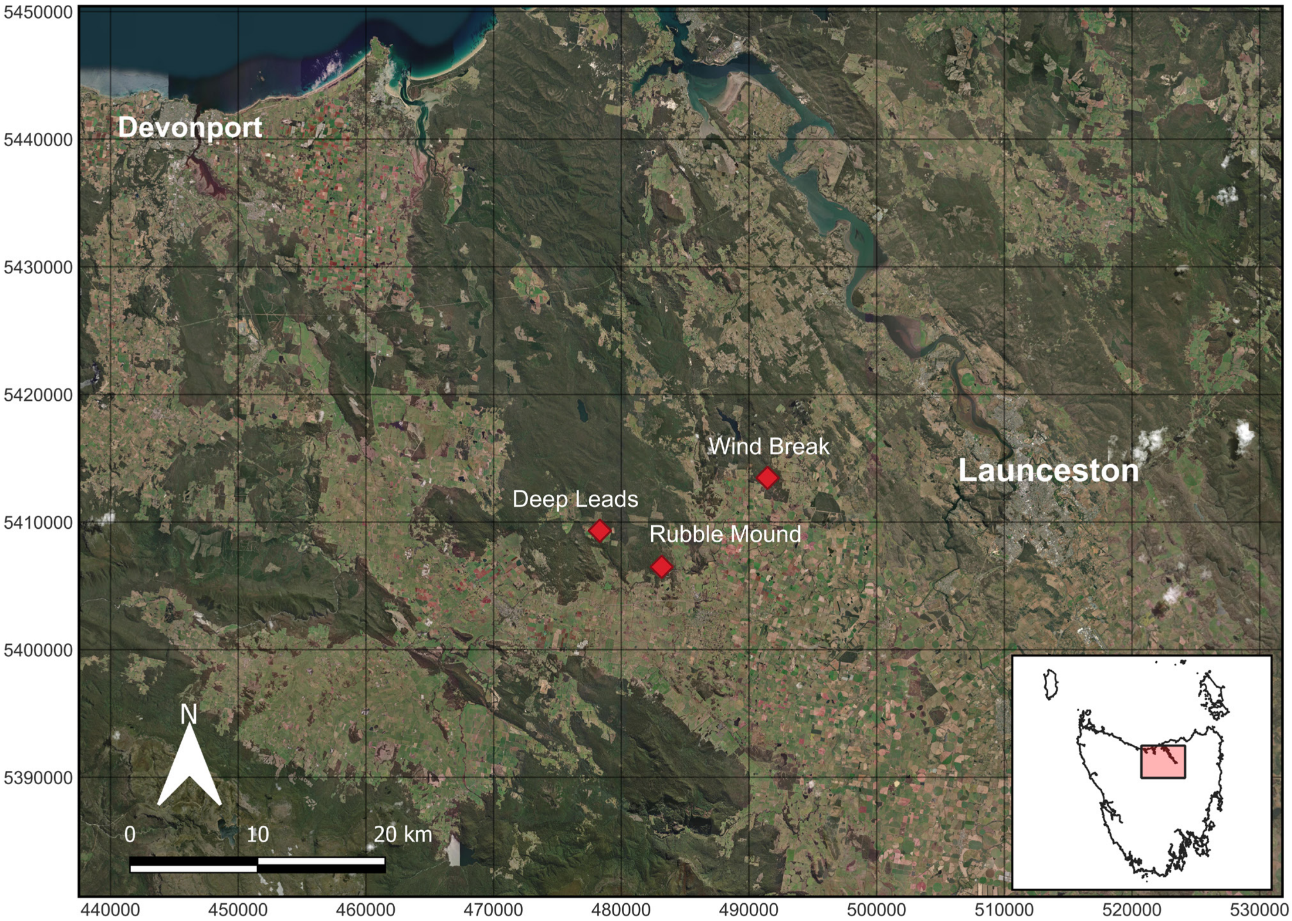

Figure 1. Location of ABx Group's Deep Leads projects in northern Tasmania.

In Australian IACD REE systems, the proportion of ionically adsorbed REEs is typically low (<10 %) relative to secondary mineral components (Knorsch, 2025). For economically viable REE extraction, higher proportions of ionically adsorbed REE components are advantageous due to their amenability to extraction via low-cost in-situ leaching under mildly acidic conditions (e.g. ammonium sulphate solutions). Metallurgical test work at Deep Leads indicates comparatively elevated ionic REE components, with in-situ leach tests yielding recoveries ranging from 24 % to 83 % using ammonium sulphate solutions at pH 4 (ABx Group, 2023).

Although typical source rocks for clay-hosted REE deposits are felsic igneous rocks (and their metamorphic equivalents) that host an abundance of REE-bearing accessory phases, examples of other clay-hosted REE deposits formed from mafic source rocks have been documented (e.g. Emeishan basalt, China; Russo et al., 2025). In Tasmania, prolonged weathering of these mafic lithologies has also led to the formation of bauxite-rich horizons within the upper portions of the regolith profile, reflecting intense leaching of silica, alkali and alkaline earth elements during lateritisation, with residual enrichment of aluminium (predominantly as gibbsite). Current mining operations by ABx Group in this region has been focused on the extraction of these bauxite-rich layers, however recent assaying for REEs has led to the discovery of clay-hosted REE mineralisation at Deep Leads. REE enrichment here is typically found to occur within clay-filled paleochannels between 2 to 5 m below surface and extends from 4 to 7 m in thickness (ABx Group, 2024).

Recent resource estimations reported by ABx Group for the project define a total mineral resource of 89 Mt at an average grade of 844 ppm total rare earth oxides (TREO) (ABx Group, 2025; Table 1). This includes elevated concentrations of heavy rare earth elements (HREE), dysprosium (Dy) and terbium (Tb) (31 ppm and 5.2 ppm respectively), with Dy+Tb proportions among the highest documented globally (ABx Group, 2023).

4.0 DRILLHOLES

A total of 242 RC drillholes were scanned using the HyLogger-3 system. The dataset comprises 186 drillholes from the Deep Leads project (includes 56 drillholes from the northern Bryans Road drilling), 30 drillholes from the Wind Break project and 26 drillholes from Deep Leads-Rubble Mound infill drilling (Figure 2). All drillholes were completed under government co-funded Exploration Drilling Grant Initiative (EDGI) programs between 2022 and 2024 (funding rounds 6 to 9), with associated geological data and reports available in the public domain (ABx Group, 2022; ABx Group, 2024). A complete list of drillholes used in this study is provided in Appendix B.

Table 1. Deep Leads clay-hosted REE deposit summary.

Deposit	Deep Leads
Latitude, Longitude	-41.5072, 146.7736
Company	ABx Group
Commodity	Rare Earth Elements
Deposit style	Ionic adsorption clay (IAC)
Source rock	Tholeiitic dolerite and alkali basalt
Age (Ma)	183
Resource and grade	89 Mt @ 844 ppm TREO
Exchangeable content %	24 - 83
References	ABx Group, 2025; ABx Group, 2023; Russo et al. 2025

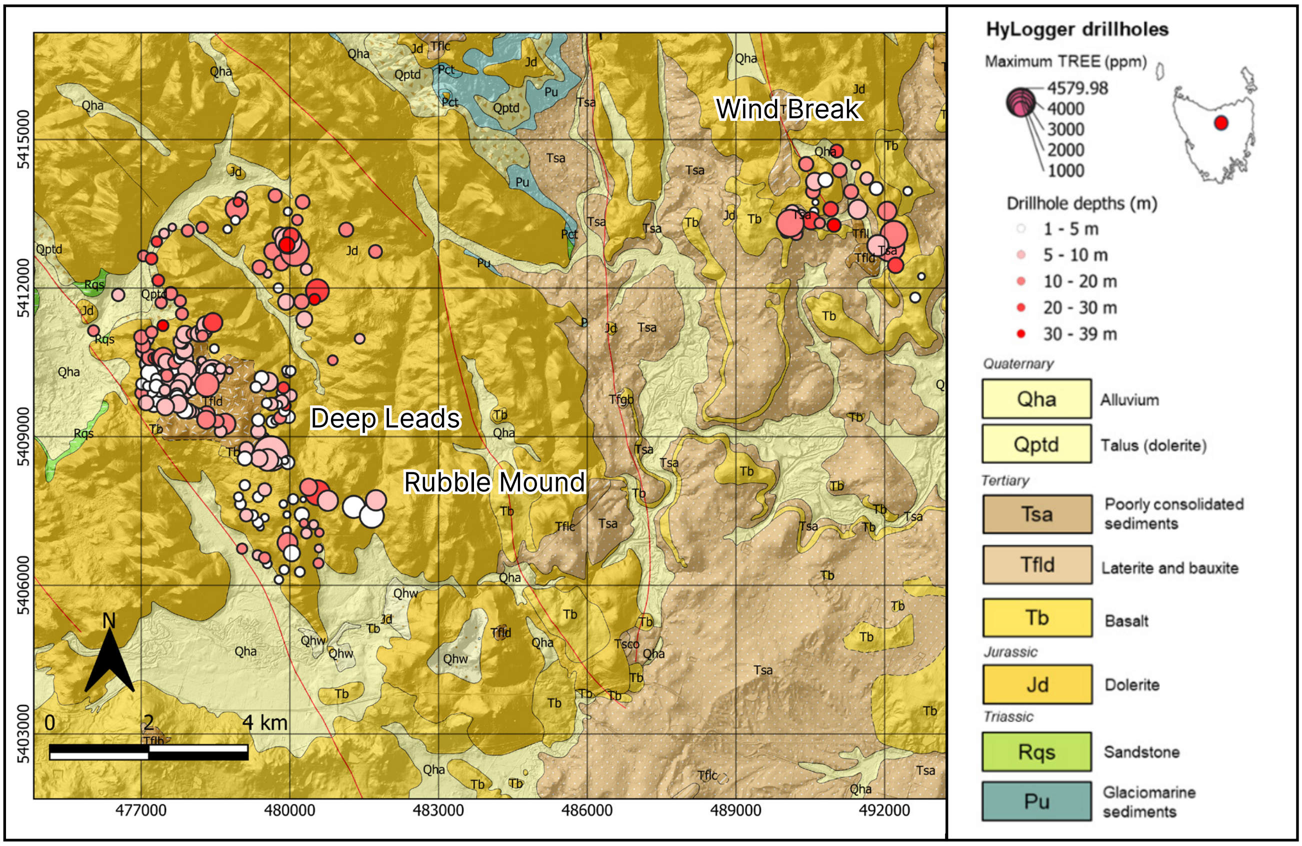

Figure 2. Locations of Deep Leads EDGI drillholes scanned with the HyLogger-3 system and used in this report (1:25 000 geology overlay).

5.0 METHODS

5.1 Geochemistry

Geochemical data used in this report were obtained from ABx Group EDGI reporting. Samples were analysed by ALS Global using the ME-MS81 method. Trace element concentrations were determined following lithium borate fusion of the sample, with subsequent analysis of the fused disc by inductively coupled plasma–mass spectrometry (ICP–MS). All analyses were subject to ALS Global internal quality assurance and quality control (QAQC) procedures.

5.2 HyLogger scanning

Hyperspectral data were acquired using the HyLogger-3 system at the Mineral Resources Tasmania Drill Core Library in Mornington, Tasmania. The instrument collects high-resolution RGB imagery and spectral data across the visible–near infrared (VNIR; 380–1000 nm), shortwave infrared (SWIR; 1000–2500 nm), and thermal infrared (TIR; 6500–14 500 nm) wavelength ranges (Schodlok et al., 2016). Drill core and RC chip trays are translated on a robotic X–Y stage beneath fixed sensors, with measurements acquired at 4 mm intervals along the centre of the samples. Each measurement has a field of view of approximately 10 × 14 mm.

Instrument calibration is maintained through routine measurements of reference materials prior to each tray scan, while daily blackbody measurements are used to calibrate TIR data to radiance. A quality control version of The Spectral Geologist (TSG-QC), coupled with an engineering monitoring program, is integrated with the HyLogger system to assess data quality and instrument performance in real time. Following each tray scan, HyLogger data are reviewed for instrument- and sensor-related error flags before subsequent trays are processed.

5.3 Data processing and interpretation

Processing and interpretation of HyLogger data was undertaken using The Spectral Geologist (TSG8) software package. Initial masking was applied to remove contaminated spectra exhibiting plastic-related features, attributed to light reflected from the walls of chip tray compartments. Spectral data from each of the three wavelength regions were processed independently. Mineral identification within the VNIR–SWIR range was performed using The Spectral Assistant (TSA) algorithm, which matches measured spectra against a validated Spectral Reference Library (Berman et al., 2011). A separate TIR Spectral Reference Library is used for the identification of minerals throughout the TIR wavelength range using the constrained least-squares (CLS) fitting algorithm (Schodlok et al., 2016; Lawson and Hanson, 1995). Results from TSG are reported as identified minerals and their corresponding modal abundances, expressed as Min1–Min3 and Wt1–Wt3, respectively. Hyperspectral data was down sampled to 1 m intervals and integrated with corresponding geochemical data in IoGAS to assess mineralogical–geochemical relationships across the study area.

6.0 HYLOGGER RESULTS

Hyperspectral data has been interpreted to characterise deposit-scale mineral distributions, REE–mineral associations, clay and Fe-oxide mineralogy and weathering profile characterisation. Given the clay-hosted nature of REE mineralisation at Deep Leads, interpretation is primarily focused on the VNIR–SWIR wavelength ranges, where clay phases and Fe-oxides are effectively discriminated.

Major mineral phases identified across Deep Leads drillholes include goethite and REE-related spectral responses in the VNIR, kaolinite (both poorly and well-crystalline), nontronite, montmorillonite, and gibbsite in the SWIR, and quartz, plagioclase, and pyroxene in the TIR. Spectral parameters have been used in this study to better understand the characteristics of these minerals (Table 2), including their association with REE enrichment, and are discussed in the proceeding sections.

6.1 REE SWIR mineral associations

Comparison of REE assay data with SWIR-derived mineralogy indicates that REE enrichment is associated with poorly-crystalline kaolinite (kaolinite-PX) at the Deep Leads project and with montmorillonite at the Wind Break project (Figures 3a, 3b). At Deep Leads, both end-member kaolinite-PX spectra and mixtures comprising >50 % kaolinite-PX correlate with the highest Total Rare Earth Element concentrations excluding cerium (TREE-Ce), typically ranging from the low hundreds of ppm up to 3113 ppm. Kaolinite-PX typically occurs in mixtures with nontronite and is commonly associated with highly-enriched zones.

Table 2. Summary of spectral parameters used in this report.

Spectral parameter	Description
Kaolinite crystallinity	A combination of the 2180 nm and 2160 nm kaolinite slope indices that correlates with kaolinite crystallinity (Pontual et al.,1997).
Kaolin composition	Measures the composition and crystallinity of kaolin group minerals ranging from kaolinite to halloysite to dickite (and nacrite) using the algorithm [(R2138+R2173)/(R2156)[(R2156+R2190)/R2173]].
Smectite index	A ratio of the deepest (AlOH, FeOH or MgOH) feature between 2160 and 2370 nm divided by the depth of the water band, between 1900 and 1990 nm. Used to separate smectites from other OH-bearing phases.
Ferric oxide abundance	Measures the depth of the Fe^{3+} (ferric iron) absorption feature near 900 nm as a proxy for ferric oxide abundance.

At Wind Break, mixtures comprising >50 % montmorillonite are typically associated with REE enrichment, including up to 2468 ppm TREE-Ce. Montmorillonite in these enriched zones typically occurs in mixtures with both well-crystalline kaolinite (kaolinite-WX) and nontronite.

Across all drillholes, well-crystalline kaolinite (kaolinite-WX) in mixtures >50 % was only associated with low to moderate REE enrichment (generally not exceeding 750 ppm TREE-Ce; Figure 3c). Gibbsite shows no association with REE enrichment, with increasing gibbsite abundance corresponding to decreasing TREE-Ce concentrations (Figure 3e).

6.2 REE-bearing VNIR spectra

Characterisation of rare earth elements (REEs) using hyperspectral data is undertaken within the visible to near-infrared (VNIR) wavelength range (380–1000 nm). Within this region, trivalent REEs exhibit diagnostic, narrow absorption features produced from electronic transitions within partially filled 4f orbitals. Most commonly, neodymium-related electronic transitions produce absorption features near 580, 740, 800, and 870 nm (Turner et al., 2014). Similar diagnostic features are documented for most REEs; however, La_2O_3, Lu_2O_3, and CeO_3 do not display distinct VNIR absorption features due to characteristics of their electronic configurations (White, 1967).

Challenges in the identification of REE absorption features can arise from several factors, including low-albedo samples and spectral interference from ferrous and ferric iron-bearing phases (Cudahy and Ramanaidou, 1997). In particular, Fe^{3+} crystal field absorption features associated with Fe-oxide minerals produces a prominent feature near 900 nm, which overlaps with diagnostic REE signatures. Analysis of REE-enriched samples from Deep Leads found that REE absorption features were inconsistently resolved. This was partly due to the persistence of goethite, which produces a moderate to deep 900 nm feature. Mafic saprolite and saprock also have inherently low reflectance and host REEs, which can further obscure REE absorption features. Although some samples exhibit prominent REE features (Figure 4), routine characterisation of REE mineralisation at Deep Leads is expected to be more reliably achieved using complementary analytical approaches. These include portable X-ray fluorescence (pXRF) for rapid screening and four-acid digest methods for comprehensive geochemical analysis.

6.3 Kaolin group

Kaolin-group minerals, including kaolinite-PX (poorly-crystalline) and kaolinite-WX (well-crystalline), are identified from SWIR data as the most abundant and widely distributed clay phases at Deep Leads. Variations in kaolinite crystallinity are characterised using both The Spectral Assistant (TSA) matching against reference spectra (e.g. kaolinite-PX and kaolinite-WX; Figure 5) and spectral indices (scalars) that quantify absorption features sensitive to structural ordering. In this study, spectral indices are favoured because they enable a more nuanced assessment of gradual changes in kaolinite crystallinity. The kaolinite crystallinity scalar quantifies the depth of the ~2160 nm absorption feature, which increases with increasing crystallinity (Pontual et al., 1997). A kaolin composition script captures compositional variation along the kaolinite–halloysite–dickite (and nacrite) series.

a)

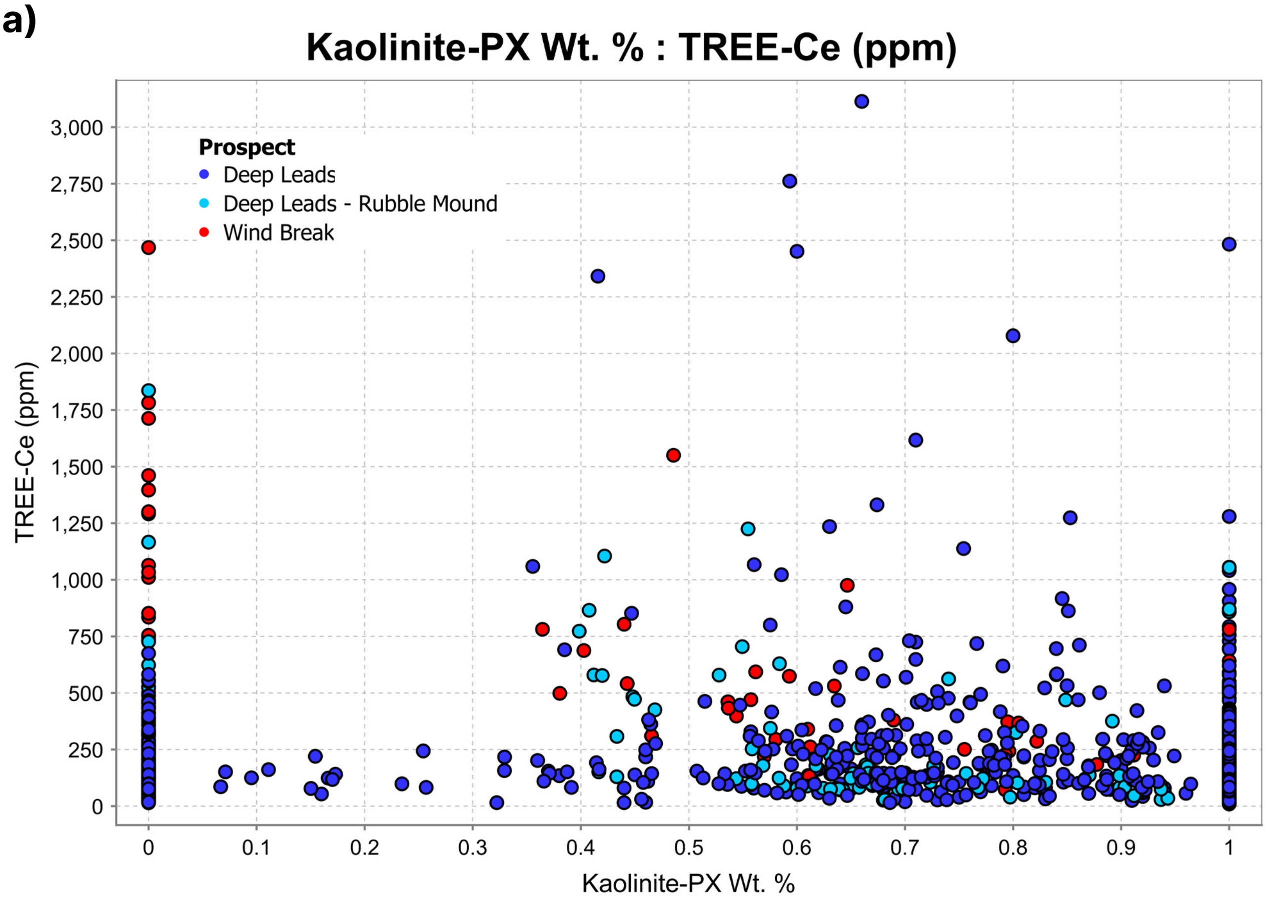
Kaolinite-PX Wt. % : TREE-Ce (ppm)
Prospect
Deep Leads
Deep Leads - Rubble Mound
Wind Break
TREE-Ce (ppm)
Kaolinite-PX Wt. %
0
250
500
750
1,000
1,250
1,500
1,750
2,000
2,250
2,500
2,750
3,000
0
0.1
0.2
0.3
0.4
0.5
0.6
0.7
0.8
0.9
1

b)

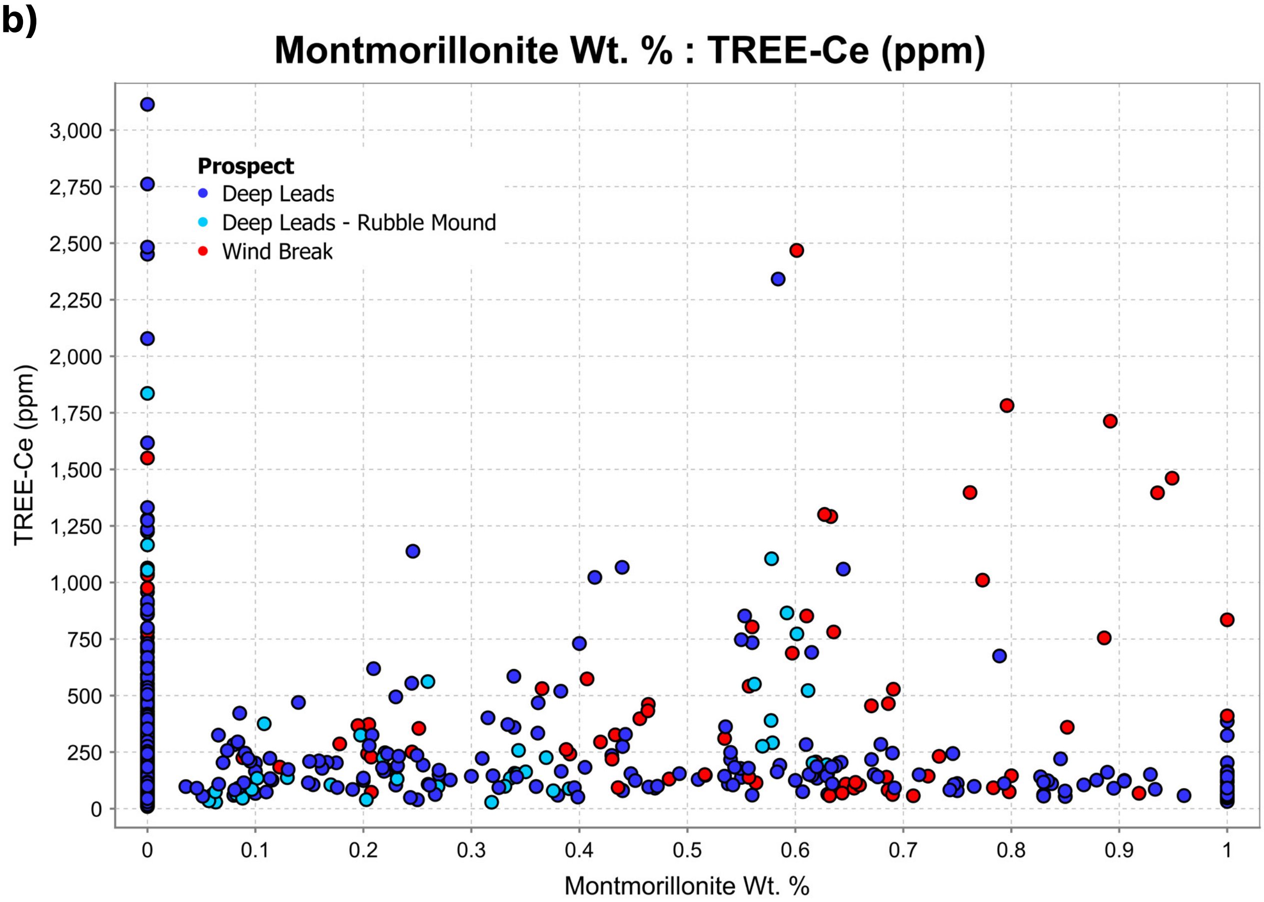
Montmorillonite Wt. % : TREE-Ce (ppm)
Prospect
Deep Leads
Deep Leads - Rubble Mound
Wind Break
TREE-Ce (ppm)
Montmorillonite Wt. %
0
250
500
750
1,000
1,250
1,500
1,750
2,000
2,250
2,500
2,750
3,000
0
0.1
0.2
0.3
0.4
0.5
0.6
0.7
0.8
0.9
1

c)

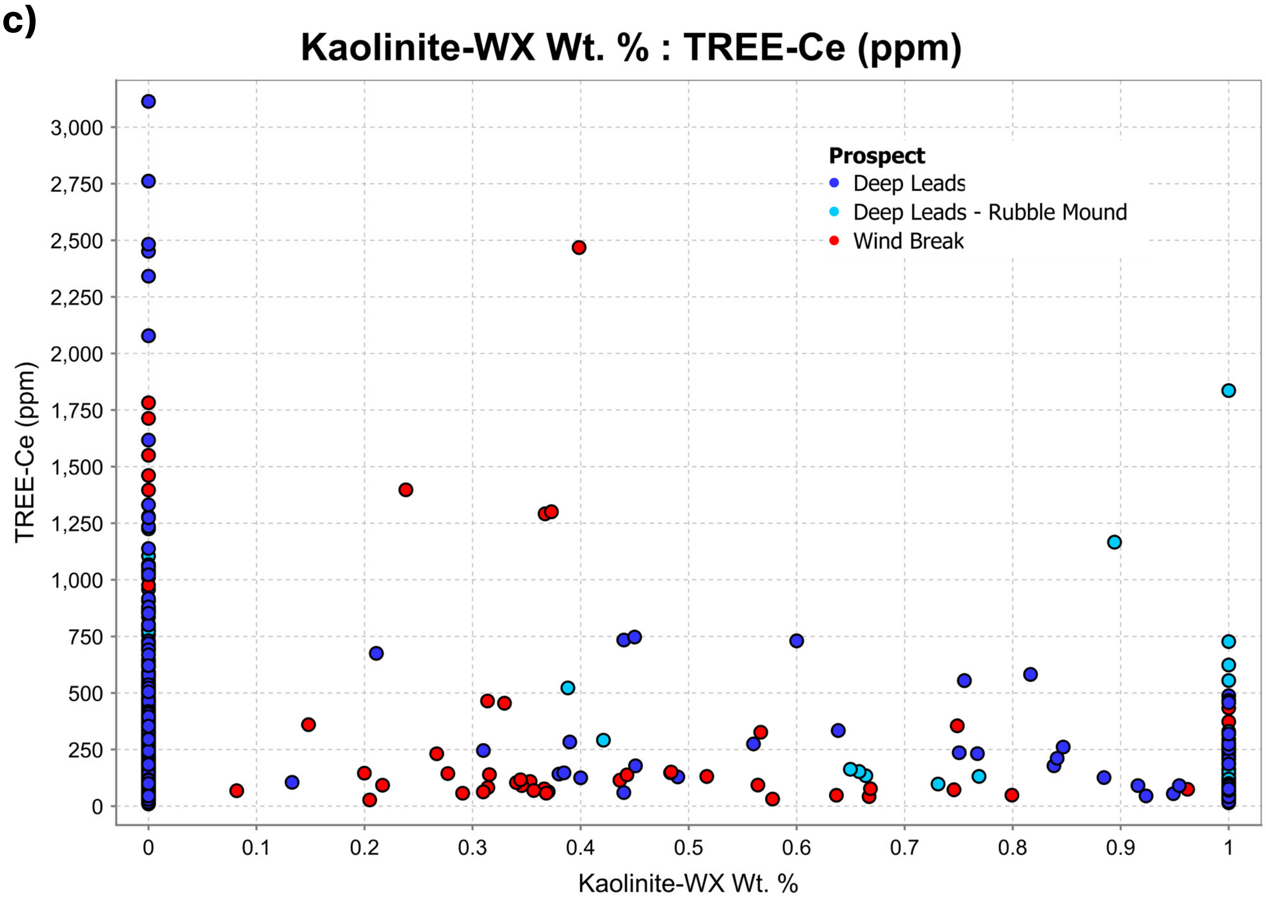
Kaolinite-WX Wt. % : TREE-Ce (ppm)
Prospect
Deep Leads
Deep Leads - Rubble Mound
Wind Break
TREE-Ce (ppm)
Kaolinite-WX Wt. %
3,000
2,750
2,500
2,250
2,000
1,750
1,500
1,250
1,000
750
500
250
0
0
0.1
0.2
0.3
0.4
0.5
0.6
0.7
0.8
0.9
1

d)

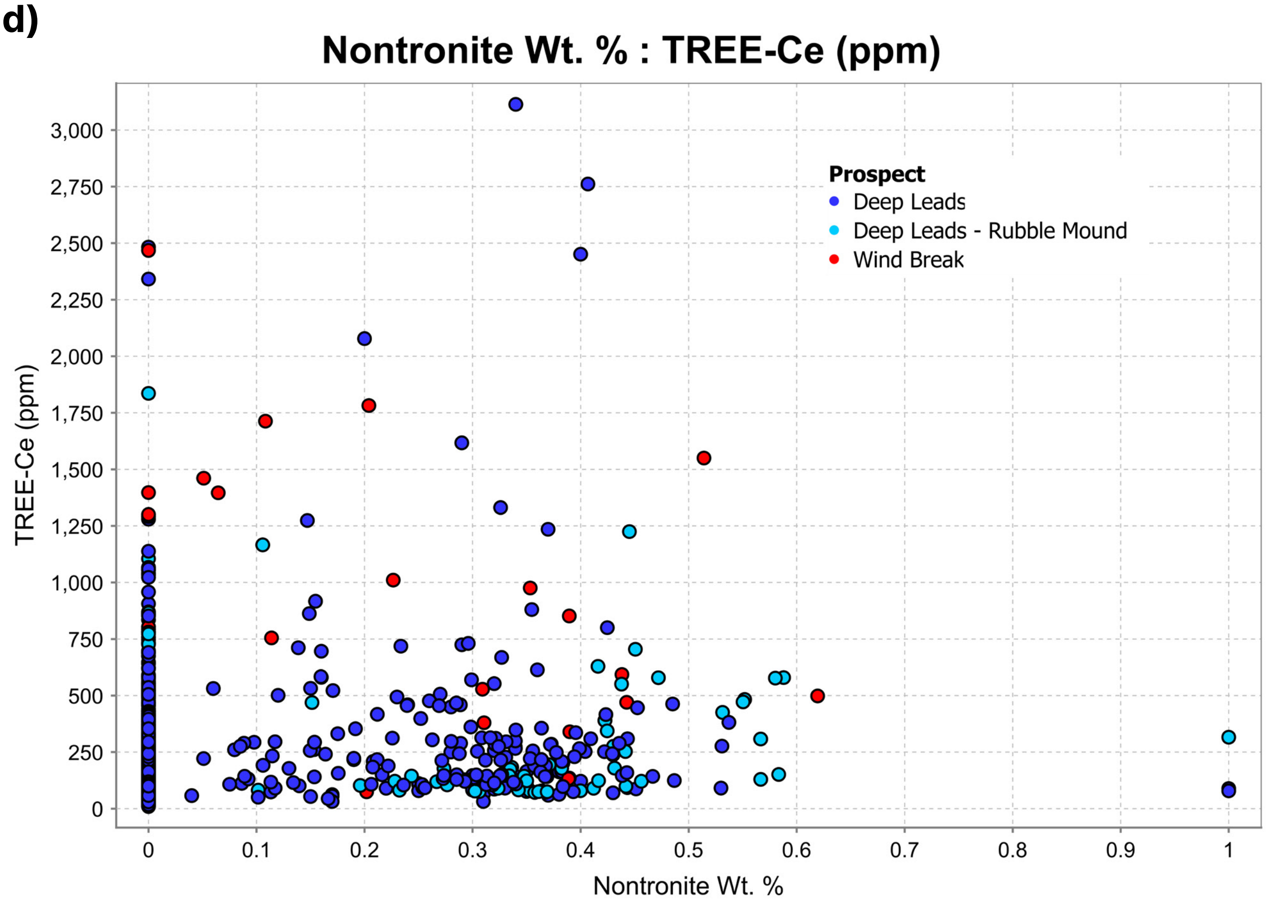
Nontronite Wt. % : TREE-Ce (ppm)
Prospect
Deep Leads
Deep Leads - Rubble Mound
Wind Break
TREE-Ce (ppm)
Nontronite Wt. %
3,000
2,750
2,500
2,250
2,000
1,750
1,500
1,250
1,000
750
500
250
0
0
0.1
0.2
0.3
0.4
0.5
0.6
0.7
0.8
0.9
1

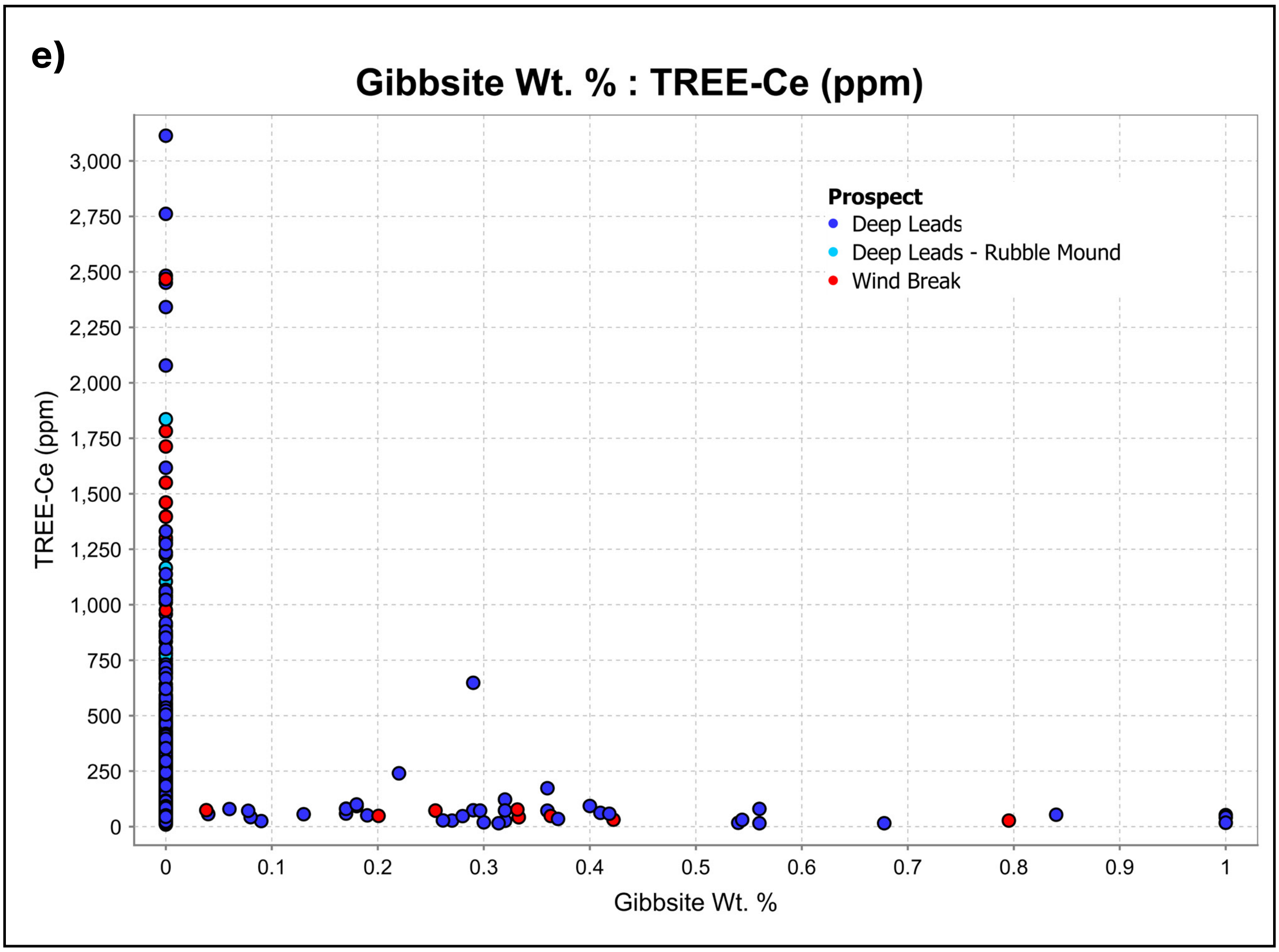

Figure 3. TREE-Ce (ppm) assay values plotted against SWIR mineral weights (a-e).

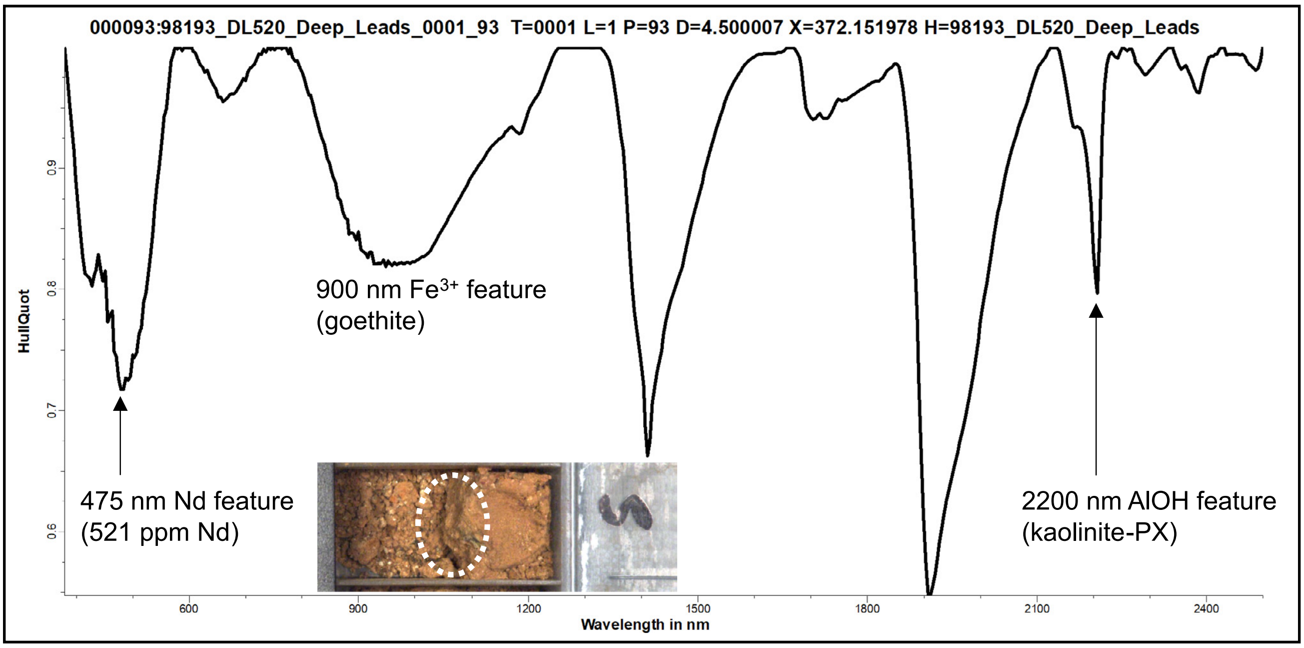

Figure 4. REE-bearing VNIR-SWIR spectra (hull-quotient) from DL520 (4 – 5 m) displaying a diagnostic 475 nm neodymium (Nd) feature (521 ppm Nd).

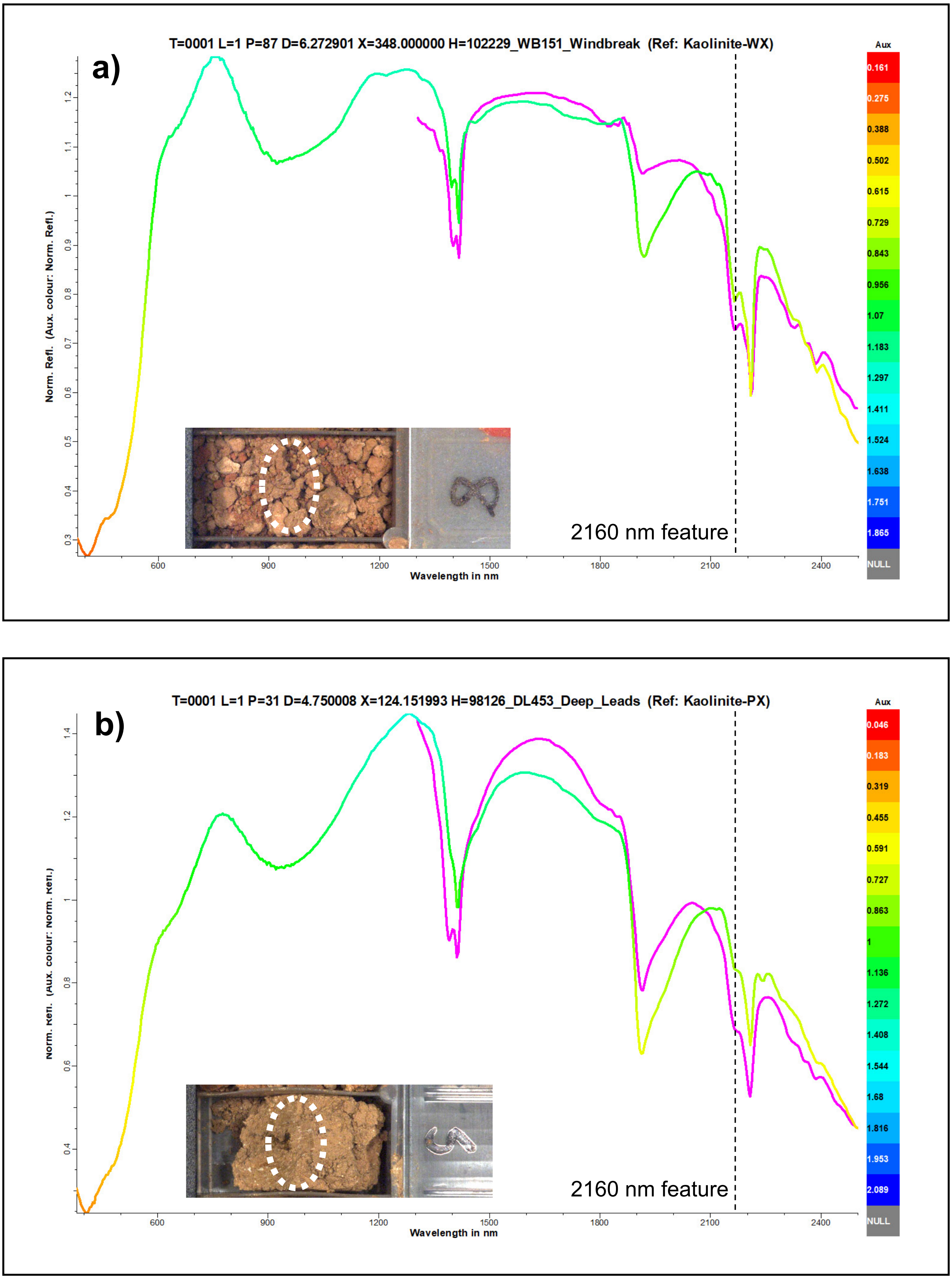

Figure 5. Comparisons between acquired spectra and kaolinite reference library spectra (purple). A) Kaolinite-WX spectra from drillhole WB151 (7 – 8 m; 68 ppm TREE-Ce). B) Kaolinite-PX spectra from the REE enriched zone of drillhole DL453 (4 – 5 m; 2078 ppm TREE-Ce). White oval denotes approximate sample location.

Comparisons between the kaolinite crystallinity and kaolin composition scalars with TREE–Ce assay data indicate that decreased kaolinite crystallinity is associated with increasing TREE–Ce grades at the Deep Leads project (Figure 6). This relationship is supported by TSA mineral matching, which identifies poorly-crystalline kaolinite (kaolinite-PX) persisting throughout REE-enriched intervals within the weathering profile and very poorly-crystalline kaolinite typically occurring near surface (0 – 2 m). In contrast, at the Wind Break project, kaolinite-PX is rarely observed in mixtures >50 % throughout REE-enriched zones.

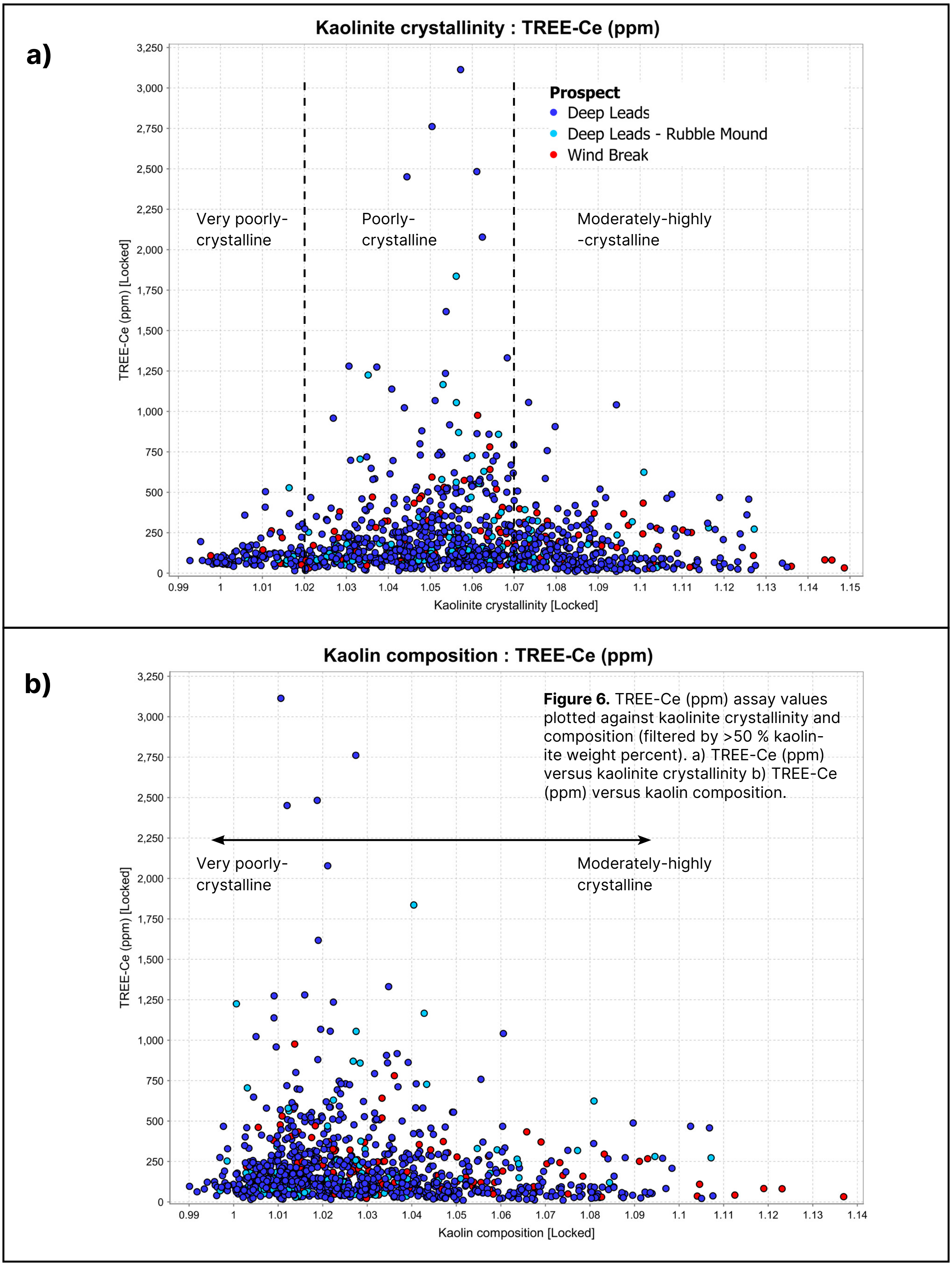

Figure 6. TREE-Ce (ppm) assay values plotted against kaolinite crystallinity and composition (filtered by >50 % kaolinite weight percent). a) TREE-Ce (ppm) versus kaolinite crystallinity b) TREE-Ce (ppm) versus kaolin composition.

6.4 Smectite group

Smectite-group minerals, identified at Deep Leads as montmorillonite and nontronite, constitute the second-most abundant clay phases after kaolinite and are widely distributed throughout the lower weathering profile. At Deep Leads, both species commonly occur as minor components within kaolinite-rich clay assemblages associated with REE enrichment. At Wind Break, increased montmorillonite abundance is associated with REE-enriched zones. The occurrence of nontronite (Fe-smectite) throughout the study area is reflective of the weathering of a mafic source rock (Figure 7a), while both nontronite and montmorillonite (2:1-layer silicates) are recognised to exhibit greater REE adsorption capacities relative to kaolinite (1:1 layer silicate).

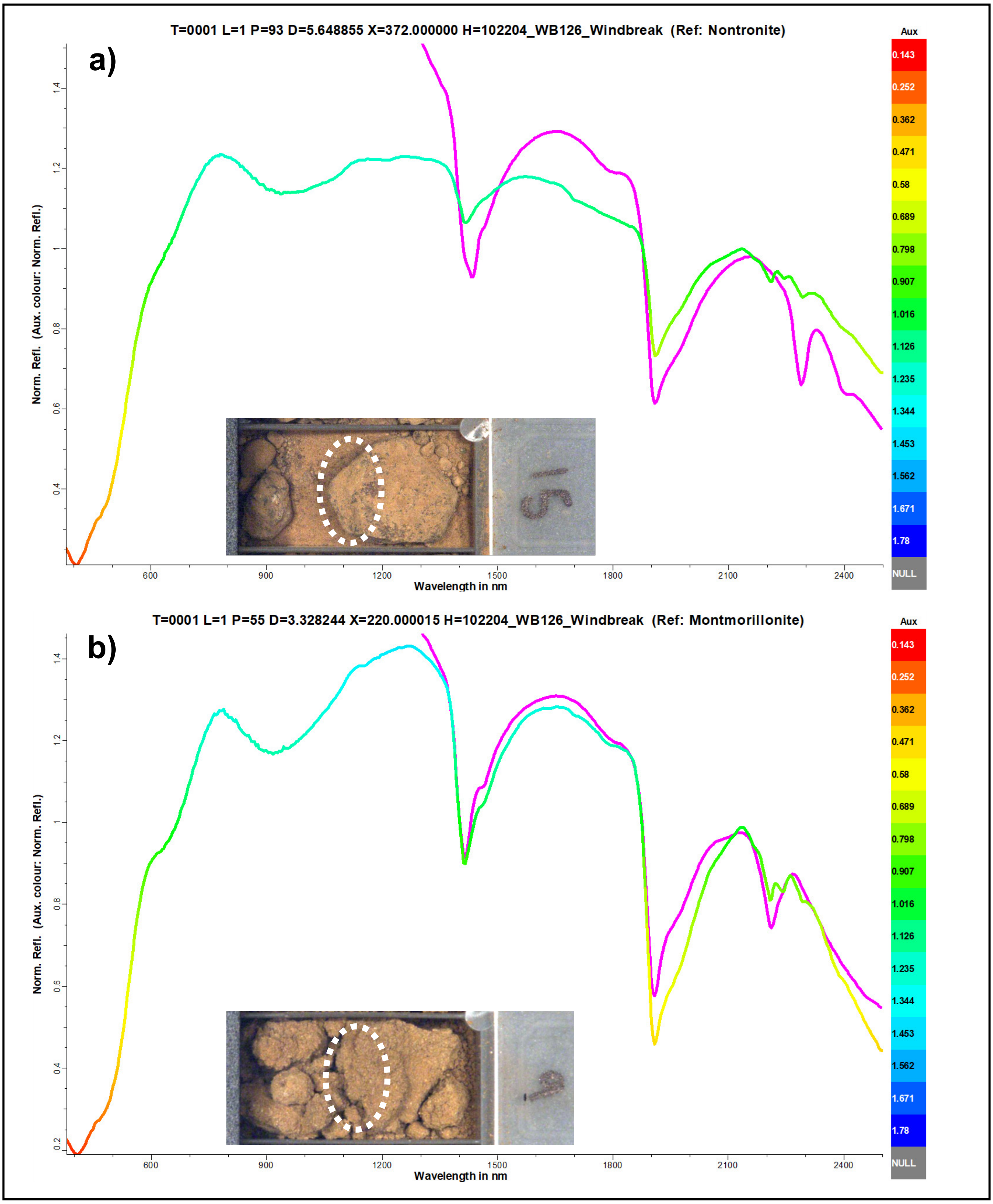

Figure 7. Comparison between acquired spectra and smectite reference library spectra (purple). A) Nontronite spectra (mixed with kaolinite-PX) from the saprock zone of drillhole WB126 (14 – 15 m; 498 ppm TREE-Ce). B) Montmorillonite spectra from the REE enriched zone of drillhole WB126 (8 – 9 m; 1782 ppm TREE-Ce). White oval denotes approximate sample location.

Application of the smectite index scalar enables discrimination of smectites from other OH-bearing minerals (e.g. kaolinite and gibbsite). The index is defined as the ratio between the ~1900 nm H_2O absorption band and the most prominent OH absorption feature (AlOH, FeOH, or MgOH). Variations in this ratio reflect differences in the relative contribution of structurally bound hydroxyl groups, versus molecular water. Higher index values are characteristic of smectites and are attributed to their 2:1 expandable crystal structure, which facilitates the incorporation of interlayer water and produces a pronounced ~1900 nm absorption feature. In contrast, lower index values are reflective of non-expandable phases such as kaolinite and gibbsite, where limited interlayer water results in a comparatively weak H_2O absorption response. Comparison of the smectite index with TREE-Ce (ppm) assay values indicates poorly-crystalline kaolinite associated with REE enrichment at the Deep Leads project and smectite (montmorillonite) at the Wind Break project (Figure 8).

6.5 Gibbsite

Gibbsite identified within Deep Leads drillholes (Figure 9) typically occurs in the upper weathering profile, where intense leaching has resulted in the residual enrichment of aluminium. These bauxitic horizons were not found to be associated with REE enrichment, particularly where they directly overlie the mottled zone, lower saprolite and saprock units that commonly host REE mineralisation. The distribution of gibbsite across the Deep Leads drillholes is notably discontinuous, likely reflecting significant spatial variability in weathering intensity and the extent of mineral leaching.

6.6 Fe-oxide group

Fe-oxide mineralogy was characterised using the VNIR spectral range (380–1000 nm). Across all analysed drillholes, goethite was identified as the sole Fe-oxide phase at Deep Leads. Discrimination between Fe-oxide species is based on the position of the diagnostic Fe^{3+} crystal field absorption feature near 900 nm, with hematite typically exhibiting absorptions at wavelengths <890 nm and goethite at wavelengths >890 nm (Rodger et al., 2022). All Fe-oxide-bearing spectra are observed to plot at longer wavelengths, consistent with goethite dominance.

The ferric oxide abundance scalar was applied to track variations in the depth of the 900 nm Fe^{3+} absorption feature, providing a proxy for relative Fe-oxide abundance. Across all prospects, comparisons between TREE-Ce assay data show increasing Fe-oxide abundance (goethite) associated with decreased REE concentrations (excluding cerium) (Figure 10). Conversely, increasing Fe-oxide abundance is shown to correlate with a relative enrichment in cerium. A decoupling of cerium from the other REEs is consistent with observations from other documented IAC REE deposits worldwide (e.g. Ambohimirahavavy, Madagascar, and Huangshe in South China; Ram et al., 2019; Lu et al., 2026) and is interpreted to reflect oxidative weathering processes ($Ce^{3+} \rightarrow Ce^{4+}$). Under these conditions, goethite promotes oxidation and strong surface retention of Ce^{4+}, leading to preferential immobilisation of cerium within the weathering profile. The more soluble REEs are mobilised and enriched in the saprolite zone (Ratié et al., 2023).

6.7 TIR mineralogy

Interpretation of TIR data was primarily undertaken to constrain regolith zone transitions, including the delineation of saprock and fresh bedrock through the identification of anhydrous silicate minerals (e.g. plagioclase and pyroxene) characteristic of mafic source rocks. Throughout the weathering profile, quartz is typically observed to persist in low abundances (generally <10 %). Accurate characterisation of plagioclase and pyroxene species proved challenging due to their low concentrations and the persistence of fine-grained material, which induces volume scattering effects and degrades diagnostic TIR spectral features. Consequently, both minerals have been classified at the group level, which we consider sufficient for the purposes of this study.

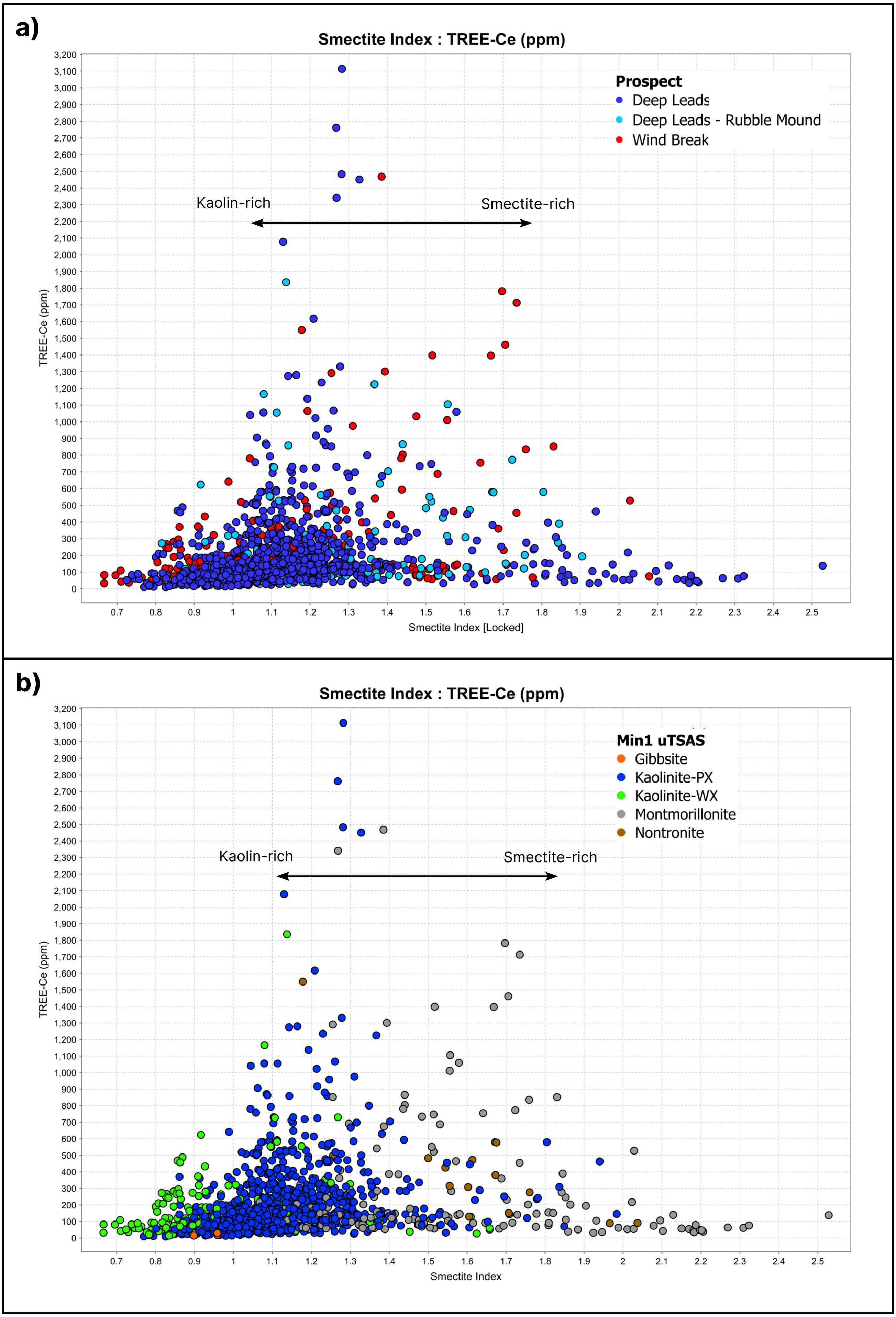

Figure 8. TREE-Ce (ppm) assay values plotted against smectite index used to discriminate smectite group minerals from other AlOH-bearing phases. A) Coloured by prospect. B) Coloured by SWIR mineral 1.

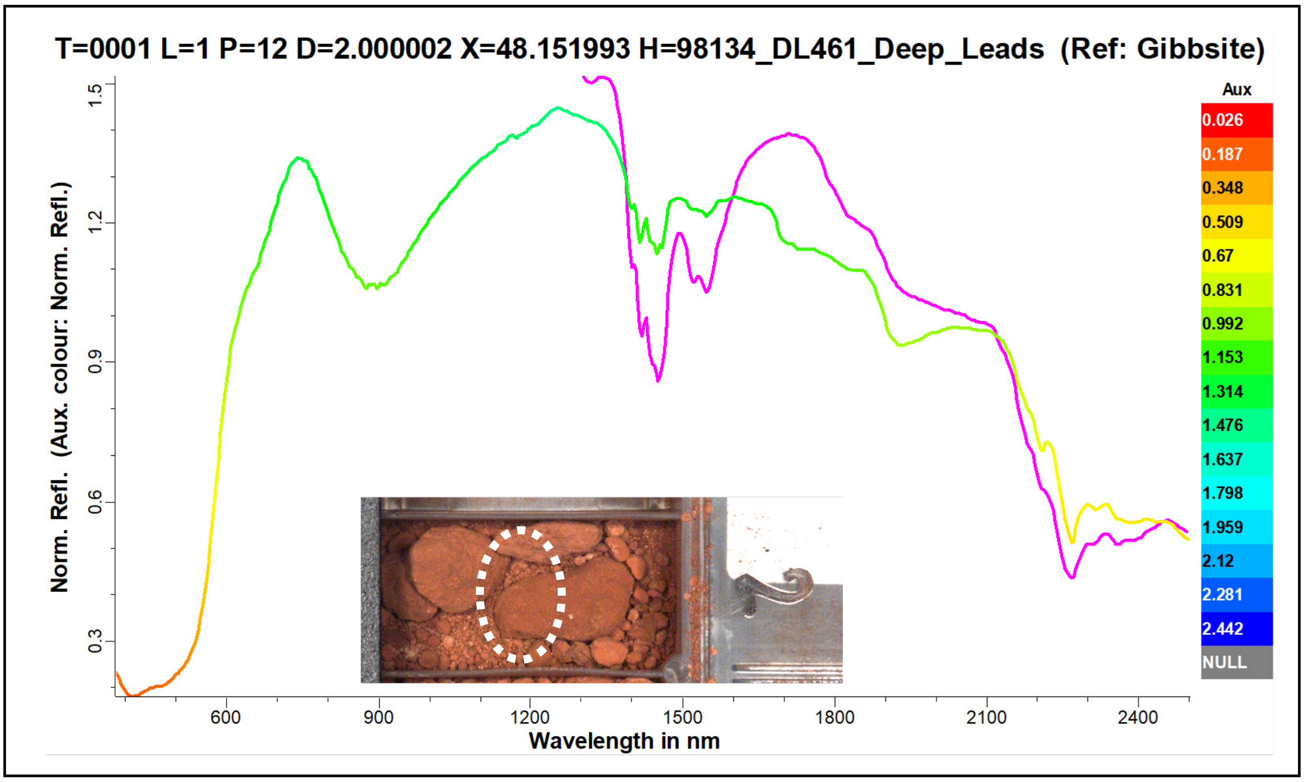

Figure 9. Comparison of gibbsite reference library spectra (purple) with spectra acquired from the upper weathering profile (1 to 2 m) of drillhole DL462 (no assay data available). White oval denotes approximate sample location.

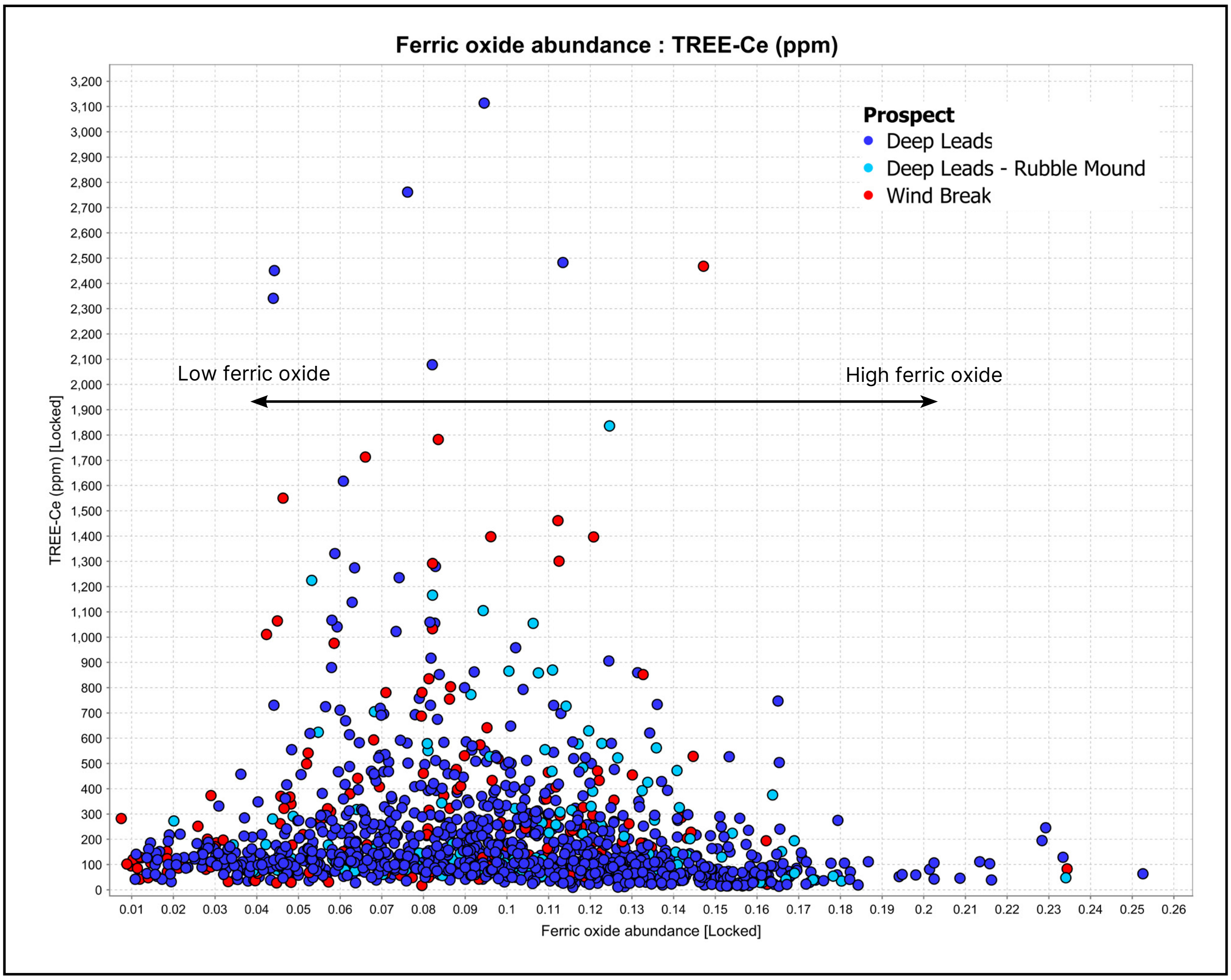

Figure 10. TREE–Ce (ppm) assay values plotted against ferric oxide abundance, used to distinguish goethite-dominated oxidised zones.

7.0 DISCUSSION

7.1 Weathering profile

Hyperspectrally-derived mineralogical data indicates that the weathering profile developed at Deep Leads is spatially highly variable in both mineralogy and thickness. This variability is expressed both laterally across the deposit and with depth to fresh bedrock. Based on the current drillhole spacing and drillholes scanned by the HyLogger, this has resulted in regolith zones which cannot be currently resolved (Figure 11). More closely spaced drillholes combined with HyLogger analysis may better resolve these weathering zones. In the drillholes examined in this study, weathering profiles are observed to extend from surface to approximately 25 m depth at both Deep Leads and Wind Break.

Variations in weathering profile development are interpreted to reflect differences in weathering intensity and leaching conditions across the study area. Notably, increased smectite abundance throughout the saprolite zone at Wind Break, and the absence of gibbsite in Deep Leads–Rubble Mound infill drillholes, indicate more reduced leaching conditions than those observed at Deep Leads. This is consistent with Mineral Resources Tasmania 1:25 000 scale geological mapping (Vicary, 2004), which shows laterite derived from dolerite more extensively developed in the Deep Leads area, and is less widely distributed at Wind Break, Deep Leads–Rubble Mound infill drilling, and Bryans Road (Figure 2).

Deeper HyLogger drillholes that capture the full weathering profile (DL468) provide a framework for characterising the regolith architecture at Deep Leads and its relationship to REE enrichment. Based on hyperspectral interpretations, a complete vertical weathering profile can be subdivided into the following regolith zones from surface to fresh bedrock:

1. Clay/soil zone: kaolinite, quartz, goethite and variable gibbsite
2. Bauxite zone: gibbsite dominant, with lesser quartz, kaolinite, and goethite
3. Mottled zone: kaolinite, quartz, goethite and variable gibbsite
4. Saprolite zone: kaolinite, quartz, goethite, and increasing smectite with depth (abundant smectite at Wind Break)
5. Saprock zone: increasing primary minerals (pyroxene, plagioclase, and quartz) with lesser kaolinite, smectite, and goethite
6. Fresh rock: Typically, dolerite, dominated by pyroxene, plagioclase, and quartz, and an absence of secondary clay minerals.

7.2 REE enrichment

REE enrichment within the weathering profile at Deep Leads can be broadly divided into two distinct zones. The upper oxidised, REE-leached zone is characterised by elevated Fe-oxide (goethite) abundance, well-crystalline kaolinite, and a positive cerium anomaly (i.e., relative depletion of TREE–Ce). A lower REE-enriched zone is characterised by reduced Fe-oxide abundance, decreased kaolinite crystallinity and enrichment in total REE (negative cerium anomaly).

Similar REE zonation patterns are observed in drillholes from Wind Break; however, these were found to be associated with higher proportions of montmorillonite, commonly mixed with nontronite or well-crystalline kaolinite, throughout the saprolite zone. At both projects, REE enrichment primarily occurs throughout the saprolite zone but may also extend into the underlying saprock (e.g. DL468).

Using hyperspectrally-derived mineralogy, spectral parameters, and assay data, a generalised weathering profile for Deep Leads has been developed. The profile summarises REE–mineralogical associations observed in REE-enriched drillholes spanning the full regolith profile (Figure 12).

7.3 Implications

The hyperspectral data presented in this report demonstrates that hyperspectral techniques can be effectively applied to resolve mineralogical distributions, clay mineral characteristics, REE associations, and regolith zonation at the Deep Leads deposit, with broader applicability to other IACD systems. This understanding has important implica-

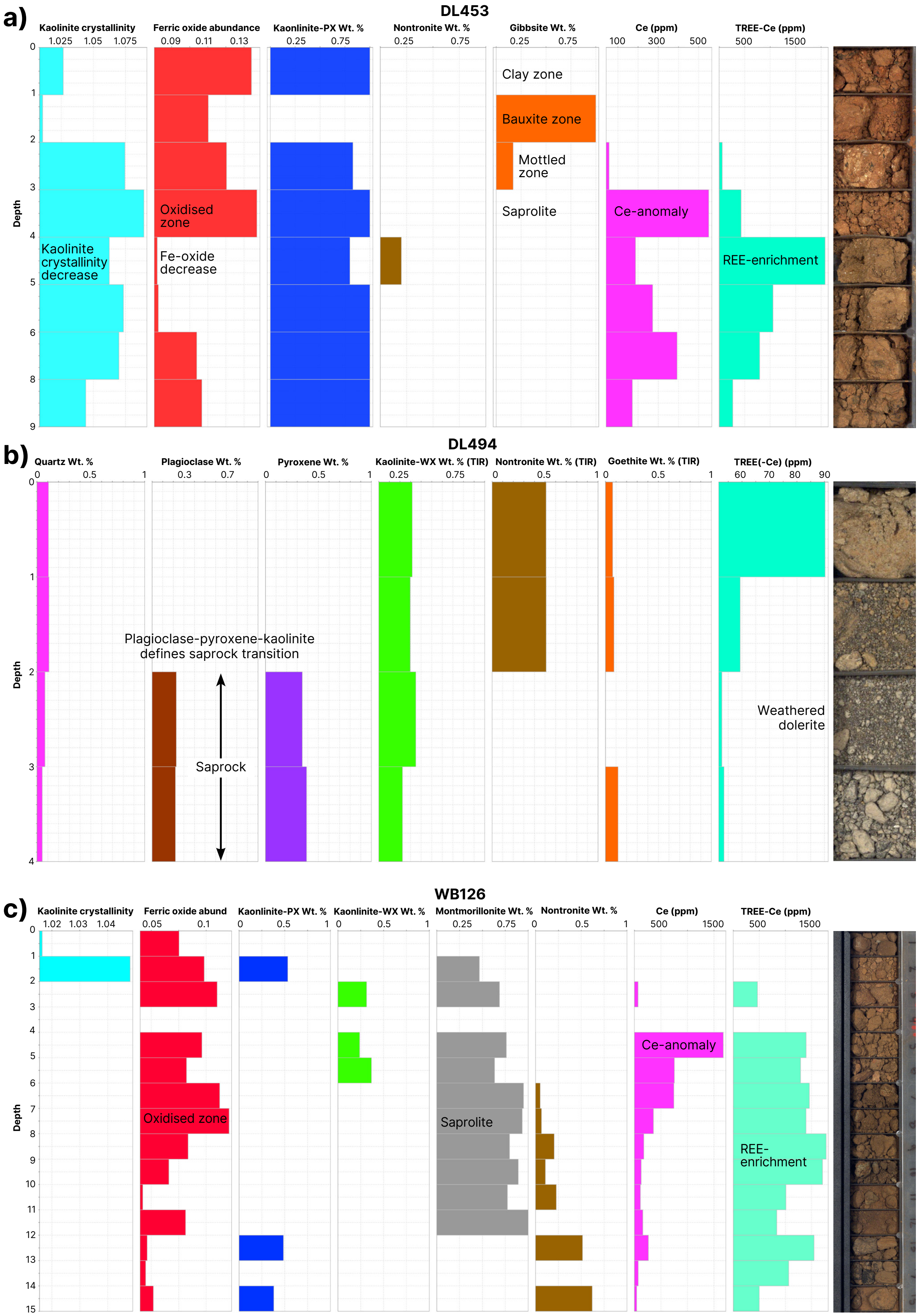

Figure 11. Downhole plots displaying hyperspectral mineralogy, spectral indices and REE assay data. a) Deep Leads drillhole DL453 with distinct regolith zonation, upper cerium anomaly and REE enrichment within the saprolite zone. b) Deep Leads drillhole DL494 with limited weathering profile development and no observable REE enrichment. c) Wind Break drillhole WB126 with REE enrichment associated with a montmorillonite-rich saprolite zone.

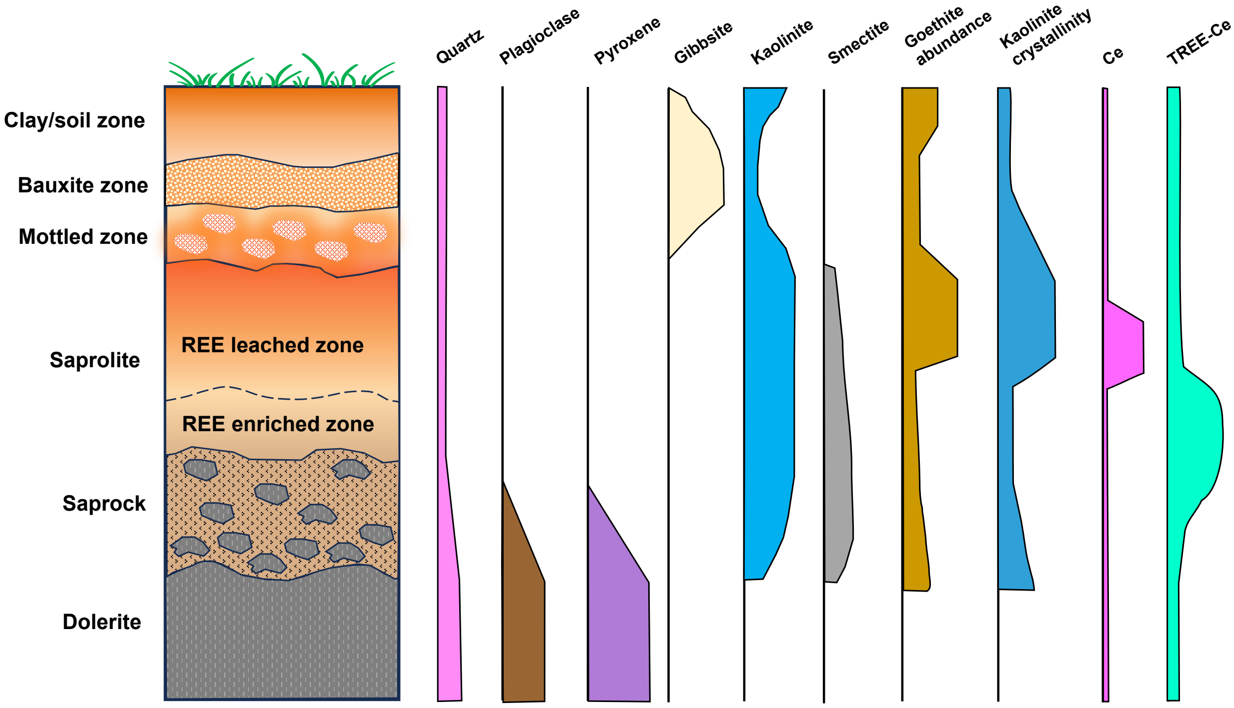

Figure 12. Generalised Deep Leads weathering profile characterised using hyperspectral and REE assay data.

tions for this style of mineralisation, particularly in relation to improving ore body knowledge. This will allow for the development of robust geological models, improve resource estimates and, notably, assist in both mineral processing and strategic mine planning. In this study, REE enrichment was found to be associated with poorly-crystalline kaolinite at Deep Leads, and with montmorillonite at Wind Break. This mineralogical characterisation may have implications for optimising REE recovery across the deposit, particularly given that montmorillonite has been reported to exhibit lower desorption efficiencies when compared to kaolinite (Alshameri et al., 2019). Further analysis is required to definitively characterise clay-hosted ionic REE components across Deep Leads (e.g. scanning electron microscopy) which is outside the scope of this study.

Although REE-related VNIR spectral features could not be reliably resolved at Deep Leads, successful prediction of REE enrichment using HyLogger datasets has been demonstrated for other IAC deposits, including the Narraburra REE deposit in NSW (Hughes and Huntington, 2025). The reduced detectability at Deep Leads is interpreted to reflect the spectral masking effects of mafic source lithologies with lower overall reflectance and high Fe-oxide abundances, which obscure REE-related spectral features. In contrast, at Narraburra, granitic source rocks with higher reflectance and comparatively lower Fe-oxide contents enhance spectral contrast and improve the detectability of REE-associated absorption features.

8.0 SUMMARY

Deposit-scale hyperspectral characterisation of RC drillholes from the Deep Leads clay-hosted REE deposit provides key insights into mineralogical controls on REE distribution and weathering profile development. The data demonstrates that hyperspectral techniques can effectively resolve clay mineralogy, REE associations and vertical zonation within this style of deposit.

Ionic components of REE mineralisation at Deep Leads may be hosted by poorly-crystalline kaolinite at the Deep Leads prospect and montmorillonite at the Wind Break prospect. A clear association between Fe-oxides and cerium is observed throughout drillholes, with decoupling of cerium from other REEs interpreted to reflect oxidative weathering processes ($Ce^{3+} \rightarrow Ce^{4+}$). Under these conditions, goethite preferentially hosts and stabilises Ce^{4+} within the weathering profile, whereas the more soluble REEs are mobilised and migrate downwards.

Prolonged in-situ weathering processes at Deep Leads have resulted in distinct vertical zonation and associated REE enrichment. An upper, oxidised and REE-leached zone is characterised by a cerium anomaly, increased Fe-oxide abundance and increased kaolinite crystallinity. A lower REE-enriched zone is defined by elevated REE (excluding Ce), reduced Fe-oxide content and poorly-crystalline kaolinite at Deep Leads and montmorillonite at Wind Break.

9.0 ACCESS THE DATA

Deep Leads TSG datasets and outputs are available in the public domain and can be accessed through the following links:

- MRT publications: https://www.mrt.tas.gov.au/home/recent-publications
- AuScope portal: https://portal.auscope.org.au/
- CSIRO NVCL portal (TSG): https://nvclstore.z8.web.core.windows.net/Tas/

10.0 ACKNOWLEDGMENTS

- T. Gallagher conducted HyLogger scanning and V. Kameniar-Sandery assisted with data processing.
- R. Sproule, S. Richardson, B. McGee and T. Czertowicz critically reviewed the report.
- ABx Group, including J. Marinelli and I. Levy, provided feedback on the study.
- C. Large edited the report and prepared it for publication.

11.0 REFERENCES

ABx Group. 2022. F*inal drilling report on work subject to an Exploration Drilling Grant Initiative (EDGI) funding – Round 6 on tenements: EL9/2010 – Deloraine and EL10/2010 – Rubble Mound (Bushy Rivulet)*. ABx Group, Sydney, NSW. https://www.mrt.tas.gov.au/exploration/exploration_drilling_grant_initiative_edgi_results/round_6.

ABx Group. 2023. *Widespread High Extractions of Ionic Adsorption Clay Rare Earths*. 02.02.2023. Australian Stock Exchange. https://cdn-api.markitdigital.com/apiman-gateway/ASX/asx-research/1.0/file/2924-02627315-2A142845.

ABx Group. 2024. *Final drilling report on work subject to an Exploration Drilling Grant Initiative (EDGI) funding – Round 9 on tenement: EL10/2021 – Brushy Rivulet (aka Rubble Mound), holes RM355 to RM458, Bryans Road Campaign*. ABx Group, Sydney, NSW. https://www.mrt.tas.gov.au/exploration/exploration_drilling_grant_initiative_edgi_results/round-9-edgi-results.

ABx Group. 2024. *Thick Dy & Tb REE results in NW Block of Deep Leads – Updated*. 08.08.2024. Australian Stock Exchange. https://abxgroup.com.au/announcements/6473416.

ABx Group. 2025. *Rare Earths Tenure Expanded in Northern Tasmania*. 12.12.2025. Australian Stock Exchange. https://abxgroup.com.au/announcements/7309142.

Alshameri, A., He, H., Xin, C., Zhu, J., Wang, X., Zhu, R., Wang, H. 2019. Understanding the role of natural clay minerals as effective adsorbents and ion exchangers for heavy metal removal. *Applied Clay Science*, 168:12–27.

Berman, M., Bischof, L., Lagerstrom, R., Guo, Y., Huntington, J., Mason, P. 2011. An unmixing algorithm based on a large library of shortwave infrared spectra. *CSIRO Technical Report*, EP117468:37.

Corbett, K. D., Quilty, P. G., Calver, C. R. 2014. *Geological Evolution of Tasmania*. Geological Society of Australia (Tasmania Division).

Cudahy, T. J., Ramanaidou, E. R. 1997. Measurement of the hematite:goethite ratio using field visible and near-infrared reflectance spectrometry in channel iron deposits, Western Australia. *Australian Journal of Earth Sciences*, 44:411–420.

Everard, J. L., Lo, C., Zhang, M. 2024. The age of Tasmanian Cenozoic basalts, determined by the 40Ar/39Ar method. *Tasmania Geological Survey Technical Report*, TR42.

Hughes, K., Huntington, J. 2025. Hyperspectral characterisation of the Narraburra REE deposit. *Geological Survey of NSW Report*, GS2025/0001.

Ivanov, A. V., Meffre, S., Thompson, J., Corfu, F., Kamenetsky, V. S., Kamenetsky, M. B., Demonterova, E. I. 2017. Timing and genesis of the Karoo-Ferrar large igneous province: New high-precision U–Pb data for Tasmania confirm short duration of the major magmatic pulse. *Chemical Geology*, 455:32–43.

Knorsch, M., Gazley, M., Ince, M., Kartal, M., Trunfull, E., Lilly, K., Piechocka, A. 2025. An introduction to clay-hosted REE deposits in Australia. *Geoscience Frontiers*, 16, 101977.

Lawson, C. L., Hanson, R. J. 1995. Solving Least Squares Problems. *Classics in Applied Mathematics*, SIAM: Philadelphia.

Lu, M., Tan, W., Liu, J., Liang, X., Brueckner, S. M., Wei, S., Yang, Y., Liu, H., He, H. 2026. Cerium speciation and anomaly formation in mature regolith: implications for ion-adsorption type REE deposit prospecting. *Geochimica et Cosmochimica Acta*, 416:139–153.

Pontual, S., Merry, N., Gamson, P. 1997. *Spectral Analysis Guides for Mineral Exploration: Vol 1 – Regolith Logging*. Auspec International Pty Ltd.

Pontual, S., Merry, N., Gamson, P. 1997. *Spectral Analysis Guides for Mineral Exploration: Vol 1 - Spectral Interpretation Field Manual*. Auspec International Pty Ltd.

Ram, R., Becker, M., Brugger, J., Etschmann, B., Burcher-Jones, C., Howard, D., Kooyman, P. J., Petersen, J. 2019. Characterisation of a rare earth element- and zirconium-bearing ion-adsorption clay deposit in Madagascar. *Chemical Geology*, 522:93–107.

Ratié, G., Zhang, K., Iqbal, M. M., Vantelon, D., Mahé, F., Rivard, C., Komárek, M., Bouhnik-Le Coz, M., Dia, A., Hanna, K., Davranche, M., Marsac, R. 2023. Driving forces of Ce(III) oxidation to Ce(IV) onto goethite. *Chemical Geology*, 633, 121547.

Rodger, A., Ramanaidou, E. R., Laukamp, C., Lau, I.C. 2022. A qualitative examination of the iron boomerang and trends in spectral metrics across iron ore deposits in Western Australia. *Applied Sciences*, 12(3), 1547.

Russo, S. C., Gonzalez-Alverez, I., Cocker, H. A., McCoy-West, A. 2025. The fundamentals of rare earth element ion adsorption clay deposits: A mineral systems approach for exploration. *Journal of Geochemical Exploration*, 278:107845.

Sanematsu, K., Watanabe, Y. 2016. Characteristics and genesis of ion-adsorption type rare earth element deposits. *Economic Geology*, 111(3):629–650.

Schodlok, M., Green, A., Huntington, J. 2016. A reference library of thermal infrared mineral reflectance spectra for the HyLogger-3 drill core logging system. *Australian Journal of Earth Sciences*, 63(8):941-949.

Schodlok, M., Whitbourn, L., Huntington, J., Mason, P., Green, A., Berman, M., Coward, D., Connor, P., Wright, W., Jolivet, M., Martinez, R. 2016. HyLogger-3, a visible to shortwave and thermal infrared reflectance spectrometer system for drill core logging: functional description. *Australian Journal of Earth Sciences*, 63(8):929-940.

Seymour, D. B., Calver, C. R. (1995) Explanatory notes for the Time–Space Diagram and Stratotectonic Elements Map of Tasmania. *Tasmania Geological Survey Record*, 1995/01.

Turner, D. J., Rivard, B., Groat, L. A. 2014. Visible and short-wave infrared reflectance spectroscopy of REE fluorocarbonates. *American Mineralogist*, 99:1335–1346.

Vicary, M. J. (compiler). 2004. *Digital Geological Atlas 1:25 000 Scale Series. Sheet 4640 Deloraine*. Mineral Resources Tasmania.

Ware, B., Jourdan, F., Timms, N. E. 2023. The Ferrar Continental Flood Basalt: A ~1.6 Ma long duration evidenced by high-precision ^40Ar/^39Ar ages suggest a potential role in the Pliensbachian–Toarcian extinction event. *Earth and Planetary Science Letters*, 622, 118369.

White, W. B. 1967. Diffuse-reflectance spectra of rare-earth oxides. *Applied Spectroscopy*, 21(3):167–171.

APPENDIX A

Data package resulting from this study

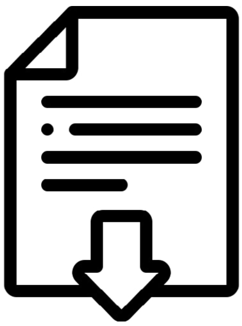

Download data

APPENDIX B

Deep Leads RC drillholes scanned with
Mineral Resources Tasmania's HyLogger-3
instrument and used in this report
(coordinates referenced to GDA94).

Prospect	Drillhole ID	Drillhole	Easting	Northing	Length (m)
Deep Leads	98104	DL438	478237	5410183	3
Deep Leads	98105	DL439	478175	5410255	7
Deep Leads	98106	DL440	478258	5410423	8
Deep Leads	98107	DL441	478217	5410528	8
Deep Leads	98108	DL442	478226	5410534	9
Deep Leads	98109	DL443	478136	5410169	8
Deep Leads	98110	DL444	477934	5409896	8
Deep Leads	98111	DL445	478038	5409943	3
Deep Leads	98119	DL446	478477	5410780	4
Deep Leads	98124	DL451	478419	5410224	8
Deep Leads	98125	DL452	478367	5410233	8
Deep Leads	98126	DL453	478427	5410293	8
Deep Leads	98127	DL454	478367	5410304	6
Deep Leads	98128	DL455	478440	5410348	8
Deep Leads	98129	DL456	478395	5410358	5
Deep Leads	98131	DL458	478606	5410377	10
Deep Leads	98134	DL461	478780	5410339	7
Deep Leads	98135	DL462	478695	5409260	15
Deep Leads	98136	DL463	478604	5409108	6
Deep Leads	98137	DL464	478540	5409313	14
Deep Leads	98141	DL468	478380	5410041	22
Deep Leads	98142	DL469	478378	5410041	15
Deep Leads	98143	DL470	478325	5410053	16
Deep Leads	98144	DL471	479490	5408990	7
Deep Leads	98145	DL472	479451	5408917	4
Deep Leads	98146	DL473	479547	5408953	6
Deep Leads	98147	DL474	479515	5408890	10
Deep Leads	98148	DL475	479537	5408808	6
Deep Leads	98149	DL476	479589	5408712	4
Deep Leads	98150	DL477	479619	5408662	7
Deep Leads	98151	DL478	479958	5408481	2
Deep Leads	98152	DL479	479898	5408518	2
Deep Leads	98153	DL480	479123	5408756	8
Deep Leads	98158	DL485	478323	5409457	12
Deep Leads	98159	DL486	478161	5409490	4
Deep Leads	98160	DL487	478057	5409505	6
Deep Leads	98161	DL488	477952	5409519	6
Deep Leads	98162	DL489	477874	5409535	5
Deep Leads	98163	DL490	477257	5409655	4
Deep Leads	98164	DL491	479979	5409401	5
Deep Leads	98165	DL492	480018	5409833	8
Deep Leads	98166	DL493	479965	5410300	6
Deep Leads	98167	DL494	479928	5410344	4
Deep Leads	98168	DL495	479743	5408499	4
Deep Leads	98169	DL496	479549	5408532	6
Deep Leads	98170	DL497	479382	5408563	6
Deep Leads	98171	DL498	479092	5408562	4
Deep Leads	98172	DL499	479363	5409108	6
Deep Leads	98173	DL500	479362	5409338	4
Deep Leads	98174	DL501	479650	5409306	4
Deep Leads	98175	DL502	479708	5409326	5
Deep Leads	98176	DL503	479805	5409385	15

Prospect	Drillhole ID	Drillhole	Easting	Northing	Length (m)
Deep Leads	98177	DL504	479891	5409527	4
Deep Leads	98178	DL505	479920	5409624	23
Deep Leads	98179	DL506	479774	5409726	5
Deep Leads	98180	DL507	479803	5409893	5
Deep Leads	98181	DL508	479871	5409990	22
Deep Leads	98182	DL509	479837	5409711	7
Deep Leads	98183	DL510	479766	5409646	5
Deep Leads	98184	DL511	479631	5409661	7
Deep Leads	98185	DL512	479533	5409680	4
Deep Leads	98186	DL513	479589	5410018	4
Deep Leads	98187	DL514	479570	5410109	6
Deep Leads	98188	DL515	477349	5409772	5
Deep Leads	98189	DL516	479429	5410188	5
Deep Leads	98190	DL517	479317	5410004	4
Deep Leads	98191	DL518	477482	5409936	25
Deep Leads	98192	DL519	477552	5410084	4
Deep Leads	98193	DL520	477720	5410126	8
Deep Leads	98194	DL521	477853	5410236	2
Deep Leads	98195	DL522	477781	5410352	12
Deep Leads	98196	DL523	477655	5410378	4
Deep Leads	98197	DL524	477492	5410407	8
Deep Leads	98198	DL525	477336	5410431	2
Deep Leads	98199	DL526	477134	5410476	5
Deep Leads	98200	DL527	477521	5410235	14
Deep Leads	98201	DL528	477892	5410396	4
Deep Leads	98202	DL529	477870	5410485	2
Deep Leads	98203	DL530	477892	5410565	9
Deep Leads	98204	DL531	477930	5410353	9
Deep Leads	98205	DL532	477830	5410093	8
Deep Leads	98206	DL533	477753	5409975	6
Deep Leads	98207	DL534	477563	5409885	1
Deep Leads	98208	DL535	477722	5409860	5
Deep Leads	98209	DL536	477732	5409840	3
Deep Leads	98210	DL537	477732	5409793	5
Deep Leads	98211	DL538	477828	5409722	2
Deep Leads	98212	DL539	477748	5409664	7
Deep Leads	98213	DL540	477489	5409606	6
Deep Leads	98214	DL541	477381	5409951	2
Deep Leads	98215	DL542	477202	5409935	2
Deep Leads	98216	DL543	477007	5409882	14
Deep Leads	98217	DL544	477202	5410181	3
Deep Leads	98218	DL545	477172	5410288	4
Deep Leads	98219	DL546	477308	5410167	3
Deep Leads	98220	DL547	477017	5410065	2
Deep Leads	98221	DL548	477135	5410023	2
Deep Leads	98222	DL549	477304	5410023	4
Deep Leads	98223	DL550	477473	5409900	1
Deep Leads	98224	DL551	477484	5409946	4
Deep Leads	98226	DL552	477479	5409939	8
Deep Leads	98227	DL553	477100	5409684	8
Deep Leads	98228	DL554	477015	5409696	2
Deep Leads	98229	DL555	478312	5409345	17

Prospect	Drillhole ID	Drillhole	Easting	Northing	Length (m)
Deep Leads	98230	DL556	479939	5407104	2
Deep Leads	98231	DL557	479942	5407427	4
Deep Leads	98232	DL558	479870	5407642	4
Deep Leads	98233	DL559	479496	5407365	4
Deep Leads	98234	DL560	479402	5407179	2
Deep Leads	98235	DL561	479358	5407237	2
Deep Leads	98236	DL562	479355	5407272	3
Deep Leads	98237	DL563	479253	5407414	5
Deep Leads	98238	DL564	479122	5407417	6
Deep Leads	98239	DL565	479004	5407641	4
Deep Leads	98240	DL566	478964	5407787	3
Deep Leads	98241	DL567	479092	5408022	4
Deep Leads	98242	DL568	479361	5407786	3
Deep Leads	98243	DL569	479493	5407931	8
Deep Leads	103370	DL614	477098	5410988	9
Deep Leads	103371	DL615	477026	5410719	8
Deep Leads	103372	DL616	477178	5410604	13
Deep Leads	103373	DL617	477254	5410588	24
Deep Leads	103374	DL618	477355	5410607	9
Deep Leads	103375	DL619	477446	5410599	19
Deep Leads	103376	DL620	477506	5410517	10
Deep Leads	103377	DL621	477041	5410843	11
Deep Leads	103378	DL622	477679	5410506	11
Deep Leads	103379	DL623	477783	5410592	3
Deep Leads	103380	DL624	477826	5410675	4
Deep Leads	103381	DL625	477876	5410754	8
Deep Leads	103382	DL626	477842	5410880	18
Deep Leads	103383	DL627	477848	5410972	11
Deep Leads	103384	DL628	477789	5410923	6
Deep Leads-Rubble Mound	98244	RM215	480019	5410329	4
Deep Leads-Rubble Mound	98245	RM216	480271	5407735	2
Deep Leads-Rubble Mound	98246	RM217	480557	5407869	23
Deep Leads-Rubble Mound	98247	RM218	480767	5407709	10
Deep Leads-Rubble Mound	98248	RM219	481291	5407584	1
Deep Leads-Rubble Mound	98249	RM220	481654	5407403	5
Deep Leads-Rubble Mound	98250	RM221	481739	5407717	10
Deep Leads-Rubble Mound	98251	RM222	480381	5407982	16
Deep Leads-Rubble Mound	98252	RM223	480595	5407065	11
Deep Leads-Rubble Mound	98254	RM224	480582	5406746	6
Deep Leads-Rubble Mound	98255	RM225	480242	5407427	3
Deep Leads-Rubble Mound	98256	RM226	479954	5406859	16
Deep Leads-Rubble Mound	98257	RM227	479037	5406740	15
Deep Leads-Rubble Mound	98258	RM228	479544	5406436	4
Deep Leads-Rubble Mound	98259	RM229	480284	5407256	13
Deep Leads-Rubble Mound	98260	RM230	480334	5407053	10
Deep Leads-Rubble Mound	98261	RM231	480481	5407227	9
Deep Leads-Rubble Mound	98262	RM232	480577	5406448	11
Deep Leads-Rubble Mound	98253	RM233	480066	5407740	4
Deep Leads-Rubble Mound	98263	RM234	480043	5406648	3
Deep Leads-Rubble Mound	98264	RM235	480039	5406649	5
Deep Leads-Rubble Mound	98265	RM236	480202	5406271	2
Deep Leads-Rubble Mound	98266	RM237	479886	5406315	4

Prospect	Drillhole ID	Drillhole	Easting	Northing	Length (m)
Deep Leads-Rubble Mound	98267	RM238	479350	5406609	9
Deep Leads-Rubble Mound	98268	RM239	479779	5406115	3
Deep Leads-Rubble Mound	98269	RM240	479491	5406554	13
Deep Leads	101978	RM355	479654	5412746	20
Deep Leads	101979	RM356	479829	5412511	17
Deep Leads	101980	RM357	480100	5412737	16
Deep Leads	101981	RM358	480333	5412380	6
Deep Leads	101982	RM359	480556	5411949	22
Deep Leads	101983	RM360	480498	5411773	31
Deep Leads	101984	RM361	480292	5411373	9
Deep Leads	101985	RM362	480239	5411728	12
Deep Leads	101986	RM363	479923	5411723	9
Deep Leads	101987	RM364	479768	5412003	5
Deep Leads	101988	RM365	479551	5412290	6
Deep Leads	101989	RM366	479386	5412420	15
Deep Leads	101990	RM367	479965	5412961	12
Deep Leads	101991	RM368	479806	5413079	10
Deep Leads	101992	RM369	480258	5413742	15
Deep Leads	101993	RM370	480151	5413378	11
Deep Leads	101994	RM371	479961	5413547	2
Deep Leads	101995	RM372	479704	5413869	14
Deep Leads	101996	RM373	479017	5413833	10
Deep Leads	101997	RM374	478930	5413600	12
Deep Leads	101998	RM375	478903	5413373	4
Deep Leads	101999	RM376	478742	5413192	5
Deep Leads	102000	RM377	478230	5413224	11
Deep Leads	102001	RM378	481137	5413182	13
Deep Leads	102002	RM379	480004	5412960	9
Deep Leads	102003	RM380	481728	5412740	11
Deep Leads	102004	RM381	480866	5410545	16
Deep Leads	102005	RM382	481410	5410980	6
Deep Leads	102009	RM386	476040	5411141	11
Deep Leads	102010	RM387	476537	5411865	8
Deep Leads	102011	RM388	479973	5412961	9
Deep Leads	102012	RM389	477045	5412651	11
Deep Leads	104180	RM435	480025	5413061	22
Deep Leads	104181	RM436	479940	5412873	33
Deep Leads	104182	RM437	478955	5413740	25
Deep Leads	104183	RM438	477002	5411012	14
Deep Leads	104184	RM439	477214	5411111	14
Deep Leads	104185	RM440	477440	5411245	39
Deep Leads	104186	RM441	477825	5411483	18
Deep Leads	104187	RM442	477789	5411742	15
Deep Leads	104188	RM443	477598	5411894	13
Deep Leads	104189	RM444	477403	5411710	20
Deep Leads	104190	RM445	477345	5412157	22
Deep Leads	104191	RM446	477210	5412596	22
Deep Leads	104192	RM447	477315	5412940	22
Deep Leads	104193	RM448	477464	5413104	8
Deep Leads	104194	RM449	477628	5413229	8
Deep Leads	104195	RM450	477940	5413162	11
Deep Leads	104196	RM451	477886	5411068	7

Prospect	Drillhole ID	Drillhole	Easting	Northing	Length (m)
Deep Leads	104197	RM452	478025	5411080	11
Deep Leads	104198	RM453	478162	5411083	10
Deep Leads	104199	RM454	478266	5411138	9
Deep Leads	104200	RM455	478308	5411250	7
Deep Leads	104201	RM456	478370	5411286	6
Deep Leads	104202	RM457	478448	5411307	24
Deep Leads	104203	RM458	478237	5411036	11
Wind Break	102204	WB126	492104	5412834	16
Wind Break	102205	WB127	492189	5413088	11
Wind Break	102206	WB128	492052	5413557	15
Wind Break	102207	WB129	491834	5414013	5
Wind Break	102208	WB130	491464	5413590	7
Wind Break	102209	WB131	490914	5413595	21
Wind Break	102210	WB132	490579	5413545	4
Wind Break	102211	WB133	490606	5413735	3
Wind Break	102212	WB134	490555	5413950	15
Wind Break	102213	WB135	490594	5414153	7
Wind Break	102214	WB136	490808	5414186	5
Wind Break	102215	WB137	490283	5413434	8
Wind Break	102216	WB138	490139	5413542	10
Wind Break	102217	WB139	490521	5413364	27
Wind Break	102218	WB140	490692	5413314	19
Wind Break	102219	WB141	490980	5413271	34
Wind Break	102220	WB142	491325	5413948	20
Wind Break	102221	WB143	491092	5414382	11
Wind Break	102222	WB144	490418	5414507	15
Wind Break	102223	WB145	491420	5414491	10
Wind Break	102224	WB146	492467	5413960	4
Wind Break	102225	WB147	491641	5414216	8
Wind Break	102226	WB148	491034	5414769	23
Wind Break	102227	WB149	490217	5413100	13
Wind Break	102228	WB150	490017	5413126	5
Wind Break	102229	WB151	490098	5413311	19
Wind Break	102230	WB152	491865	5412860	6
Wind Break	102231	WB153	492224	5412462	21
Wind Break	102232	WB154	492745	5412238	4
Wind Break	102233	WB155	492618	5411812	3

Tasmanian Government

Mineral Resources Tasmania
PO Box 56 Rosny Park
Tasmania Australia 7018

Phone: +61 3 6165 4800
Email: info@mrt.tas.gov.au
Web: www.mrt.tas.gov.au